PWM CURRENT SOURCE INVERTER FED INDUCTION MOTOR DRIVE

A Project Report

submitted by

NAINAR GURU SRINIVAS

in partial fulfilment of the requirements
for the award of the degree of

MASTER OF TECHNOLOGY

DEPARTMENT OF ELECTRICAL ENGINEERING
INDIAN INSTITUTE OF TECHNOLOGY MADRAS.

MAY 2015

THESIS CERTIFICATE

This is to certify that the thesis titled **PWM CURRENT SOURCE INVERTER FED INDUCTION MOTOR DRIVE**, submitted by **NAINAR GURU SRINIVAS**, to the Indian Institute of Technology, Madras, for the award of the degree of **MASTER OF TECHNOLOGY**, is a bona fide record of the research work done by him under our supervision. The contents of this thesis, in full or in parts, have not been submitted to any other Institute or University for the award of any degree or diploma.

Dr. Kamalesh Hatua

Assistant Professor

Dept. of Electrical Engineering

IIT-Madras, 600 036

Place: Chennai

Date: 06 May, 2015

ACKNOWLEDGEMENTS

It gives me immense pleasure to express my sincere and heartfelt gratitude to Dr.Kamalesh Hatua for his excellent guidance, motivation and constant support throughout the project. I consider myself extremely fortunate for having a chance to work under his supervision. In spite of his hectic schedule, he was always approachable and took his time off to discuss problems and give his advice and encouragement. I am also grateful for the laboratory facilities provided by him in the Power Electronics Simulation Laboratory and the Machines Laboratory, Department of Electrical Engineering, which facilitated my work.

I am grateful to Dr. Krishna Vasudevan for his constant support throughout the project. I also thank Dr. Lakshminarasamma and Dr. Srirama Srinivas for their help and support throughout the project.

I thank Mr. Kothandaraman and Ms. Jayasudha for their help and advice in arranging the hardware setup. I also thank Mr. Pandian and Mr. Balaganesh and all other staff of the Central Fabrication Facility for their help during the hardware setup.

I thank Mr. Saravanan and Mr. Kedarnath for their advice and constant help throughout the project.

My appreciation to my fellow students in Power Electronics Laboratory, especially Pratap for spending their valuable time in discussing the project. I would also extend my thanks to Vamsi, Jose, Anvar, Rajendranath, Venkateswarlu, Ramana Reddy, Anshad, Hridya and Parthasarathy.

ABSTRACT

KEYWORDS: Sensorless field oriented control, space vector pulse width modulation, current source inverter, induction motor

Field oriented control technique is widely used in industry for high dynamic performance variable voltage and variable frequency drive. In Field oriented control technique, stator currents of induction motor can be decomposed into two orthogonal components. Independent control of flux and speed is possible in field oriented control by controlling two orthogonal components of stator currents. Field oriented control technique provides excellent dynamic response and speed response similar to that of DC motor. Sensorless operation of induction motor implies the estimation of speed and rotor flux from stator current and voltage.

In this project, design and implementation of sensorless field oriented control of current source inverter fed induction motor drive has been carried out. A two-level current source rectifier used for this drive. The proposed drive is intended for sub-sea mining application. The DC link current is controlled by a SCR based rectifier. Space vector pulse width modulation technique is adopted to improve dynamic response and power quality of the drive. The complete hardware is developed in the laboratory. The proposed control technique is implemented in TMS320F28335 digital platform.

TABLE OF CONTENTS

LIST OF TABLES

LIST OF FIGURES

ABBREVIATIONS

PWM	Pulse Width Modulation
FOC	Field Oriented Control
CSI	Current Source Inverter
VSI	Voltage Source Inverter
LCI	Load Commutated Inverter
SVPWM	Space Vector Pulse Width Modulation
MI	Modulation Index
SCR	Silicon Controlled Rectifier
CSR	Current Source Rectifier
VFD	Variable Frequency Drive
DC	Direct Current
AC	Alternating Current
MV	Medium Voltage
PI	Proportional-Integral
IGBT	Insulated Gate Bi-polar Transistor
MOSFET	Metal Oxide Semi-conductor Field Effect Transistor
IGCT	Insulated Gate Commutated Thyristor
GTO	Gate Turn Off thyristor
THD	Total Harmonic Distortion
MMF	Magneto-Motive Force
DSC	Digital Signal Controller
IM	Induction Motor
RAM	Random Access Memory
ROM	Read Only Memory
DMA	Direct Memory Access
ALU	Arithmetic Logic Unit
CPU	Central Processing Unit
FPU	Floating Point Unit

PIE	Peripheral Interrupt Expansion
ePWM	Enhanced Pulse Width Modulation
ADC	Analogue Digital Conversion
eCAP	Enhanced Capture
eQEP	Enhanced Quadrature Encoder Pulse
CAN	Controller Area Network
I2C	Inter Integrated Circuit
SCI	Serial Communication Interface
SPI	Serial Peripheral Interface
McBSP	Multichannel Buffered Serial Port
GPIO	General Purpose Input Output
MAC	Multiply and Accumulate
SARAM	Single Access Random Access Memory
OTP	One Time Programmable
SOC	Start Of Conversion

NOTATION

v_{sr}, v_{sy}, v_{sb}	Instantaneous voltages in ryb reference frame
i_{sr}, i_{sy}, i_{sb}	Instantaneous currents in ryb reference frame
$v_{s\alpha}$, $v_{s\beta}$	Instantaneous voltages in $\alpha\beta$ reference frame
$i_{s\alpha}$, $i_{s\beta}$	Instantaneous currents in $\alpha\beta$ reference frame
i_{sd}, i_{sd}	Instantaneous currents in synchronously rotating reference frame
I_{mr}	Rotor magnetizing current
N_{se}	Equivalent number of turns in stator
N_{re}	Equivalent number of turns in rotor
F_s	Stator MMF
F_r	Rotor MMF
I_{dc}	DC link current
C_f	Filter capacitance
L_s	Source inductance
L_{dc}	DC link series inductance
R_{dc}	DC link resistance
R_s	Stator resistance per phase
R_r	Rotor resistance per phase
L_{ls}	Stator leakage reactance per phase
L_{lr}	Rotor leakage reactance per phase
L_m	Magnetizing reactance per phase
ω_{mr}	Synchronous speed
ω_{slip}	Slip speed
m_d	Torque developed
m_l	Load torque
J	Moment of inertia of induction motor
B	Frictional co-efficient of induction motor
$\psi_{s\alpha}$, $\psi_{s\beta}$	Stator flux in $\alpha\beta$ reference frame
$\psi_{r\alpha}$, $\psi_{r\beta}$	Rotor flux in $\alpha\beta$ reference frame

ρ_{mr}	Rotor flux position
K_{pi}	Proportional gain
K_i	Integral gain
T_r	Rotor time constant
G_{conv}	Gain of the converter
T_s	Switching time period
m_a	Modulation index
μ	Overlapping angle

CHAPTER 1

INTRODUCTION

The invention of the induction motor has been independently done by Galileo Ferraris and Nikola Tesla in 19^{th} century. An induction motor can be defined as three-phase, self-starting and constant speed ac motor. It is a constant speed motor, as the speed depends on the frequency of the supply and the number of poles of the motor. Earlier the usage of the induction motor was limited, due to limitation in controlling the speed of the motor. Evolution of power electronics lead to revolutionary changes in the field of electric drives. The technology advancements in the semiconductor devices such as Thyristors, MOSFETs, Insulated Gate Bipolar Transistor (IGBT), Insulated Gate Commutated Thyristor (IGCT) lead to the increasing usage of the high power medium voltage drives in the areas of mining, petro-chemical, steel, transportation and many other industries. Sub-sea mining is one of the applications of variable frequency drives.

Sub-sea mining is mineral retrieval process from the sea bed. Ocean is a combination of physical, chemical, biological and geological processes which sometimes result in valuable minerals. When the hydrothermal vents explode, chemical rich fluids will be poured up from the vents. This makes the ocean a natural repository for various minerals such as gold, silver, copper, zinc, manganese, cobalt and many more. These mineral deposits are mined using hydraulic pumps or bucket systems and are brought to the surface for further processing.

This project is for developing sub-sea mining mechanism for a depth of 6 to 7kms from the ocean surface. It is intended to use a 250KW induction motor drive for pumping out the nodules from the sea bed. The motor is placed on the ocean bed and the currents are fed to the motor through the cables from the Current Source Inverter (CSI) running all the way from surface of the ocean to the ocean bed. Generally, at 250KW power level, a Low Voltage (LV) i.e., 440V/690V drive is used. But in this application, a Medium Voltage (MV) i.e., (3.3KV/6.6KV) drive has been selected. Due to the choice of MV drive, the current drawn by the motor is reduced to a large extent. As a result, the cost of the cable is reduced.

1.1 Brief review of existing MV drives

Usually MV drives handle power ranging from 0.4MW to 40MW with terminal voltages ranging from 2.3kV to 13.8kV. Load commutated inverter (LCI) fed synchronous machines are generally used for higher power ranges of above 10MW. The semiconductor devices used are SCR, GTO, IGCT and IGBT are used for MV drives. Among all the semiconductor devices, SCR can handle maximum power. Maximum ratings of SCR ranges from 12kV/1.5kA or 4.8kV/5kA. Ratings of GTO and IGCT are of 6kV/6kA. Ratings of IGBT are of 6.5kV/0.6kA or 1.7kV/3.6kA are available.

The popular technologies for MV drives are,

1. LCI fed synchronous motor drive.
2. Cycloconverter fed induction and synchronous motor drive.
3. PWM-CSI fed induction motor drive.
4. Multilevel VSI fed drives.
5. Cascaded H-bridge fed drives.

1.1.1 LCI fed synchronous motor drive

For higher power applications of greater than 10MW, LCI fed synchronous motor drives are popular due to simplicity, reliability of power hardware and availability of higher rating thyristors. In this drive, the field winding of the synchronous machine is over-excited to ensure leading power factor at the machine terminals. Thus thyristor switches of the LCI are turned off without the help of any external communication circuits.

1.1.2 Cycloconverter based induction and synchronous motor drives

Cycloconverter fed AC drives find applications in high power (>10MW) low speed applications. The drive is widely used in steel rolling mills and ball mills in cement industry. The cycloconverter is a circuit which uses the SCR to convert AC power of one frequency into AC power at another frequency (usually limited to 1/3rd of input frequency). The main advantage of the cycloconverter is that SCR turn off is achieved by the process of line commutation. When a particular thyristor is turned on, it automat-

ically turns off previously conducting thyristor by applying a reverse voltage across the thyristor. The major drawbacks of cycloconverter based drives are the complex power structure and its limited speed range of operation.

1.1.3 PWM CSI fed induction motor drive

The PWM CSI fed induction motor drives work well in the range of (1-10) MW. The load commutation of thyristor switches is not possible in CSI fed induction motor drives. Therefore, GTO and IGCT are ideal for CSI fed drives. These switches can be turned off by the negative gating pulses. Though SCR's are cheap, rugged and can handle more power than GTO and IGCT, they are not used because they cannot be turned off by controlling the gating pulses. The CSI drive is simple in power structure. It has inherent four-quadrant operation and reliable short circuit protection capabilities.

The PWM CSI fed drive does not require any additional filter to deliver sinusoidal voltage and current to the motor. The filter is inherent into the drive. The CSI drive does not require any compensation loop for line inductance. Therefore the drive is well suited for applications where long cable is required between converter and motor. PWM CSI fed drive is an automatic choice for sub-sea mining application.

1.1.4 Multilevel VSI fed induction motor drive

With the advent of IGBT, the voltage source inverter technology became popular and slowly replaced the CSI technology for low power drives. For MV drives with machine voltage rating upto 4.16kV, the VSI technology is popular in industry. In MV drives, multilevel VSI (3 level) is commonly used for better THD and lower dv/dt stress on the machine winding compared to two-level VSI.

1.1.5 Cascaded H-bridge fed drive

Cascaded H-bridge can be used for still larger voltages (13.8kV) without any output side transformer. In this topology, each phase is powered by several full bridge cells connected in series. But this power topology requires complex input side transformer

design, bulky DC bus capacitors for every half bridge module and high switch count. Also this drive does not have regeneration capability.

1.2 CSI fed Induction Motor Drive

PWM CSI fed drive [1] is well suited for sub-sea mining applications among all of the above technologies available for MV drives. The reasons for choosing a CSI fed induction motor drive for sub-sea mining application are as follows,

1. PWM CSI feeds sinusoidal voltages and currents to the motor. Voltage doubling phenomenon at the motor winding end is absent due to sinusoidal nature of the motor voltage. In a VSI fed drive, this is a common phenomenon.
2. In PWM CSI drive line filter comes as a part of the drive. Therefore, no additional filter is required for the drive. For a VSI fed drive an additional filter would have been required to achieve sinusoidal voltage at the motor end.
3. The line inductance drop needs to be accounted in stator current controller design for VSI fed drive. Whereas in CSI fed drive, the line inductance drop need not to be considered, as line inductance comes in series path of the stator current flow. In sub-sea drive, the line inductance will be high and difficult to measure. Therefore for better controllability, CSI fed drive is chosen. In this context, the capacitive coupling is ignored.
4. PWM CSI fed drive has sufficient dynamic response required for sub-sea mining.

The various requirements and challenges in developing a MV PWM-CSI drive are as follows,

1. Enhancing power quality at line side converter.
2. Design of motor side converters.
3. Constraints of switching devices.

1.2.1 Current Source Inverter

Ideally Current Source Inverter is expected to supply balanced three-phase variable frequency current to the load. A simple two-level 3-phase current source inverter consists

of 6 semiconductor switches. Each switch should be capable of blocking bi-directional voltages and allow flowing unidirectional current. Two such switches connected in series form a leg of the inverter. 3 such legs are present in a PWM-CSI fed drive. Figure 1.1 depicts the simple power circuit diagram of a CSI fed drive. S_{i1}, S_{i3}, S_{i5} comprises top commutation group and S_{i2}, S_{i4} and S_{i6} comprises bottom commutation group. A controlled DC current source is connected at the input terminal of the CSI. Three phase supply is derived from R,Y and B terminals of the CSI as shown in the figure 1.1. Three phase capacitors (C_f) connected just across the output terminal of the CSI ensure safe commutation of the switches and sinusoidal motor currents and voltages. In real practice each switch can be realized with symmetrical blocking IGCT but in the lab experiment the switch is realized as IGBT with a series connected diode.

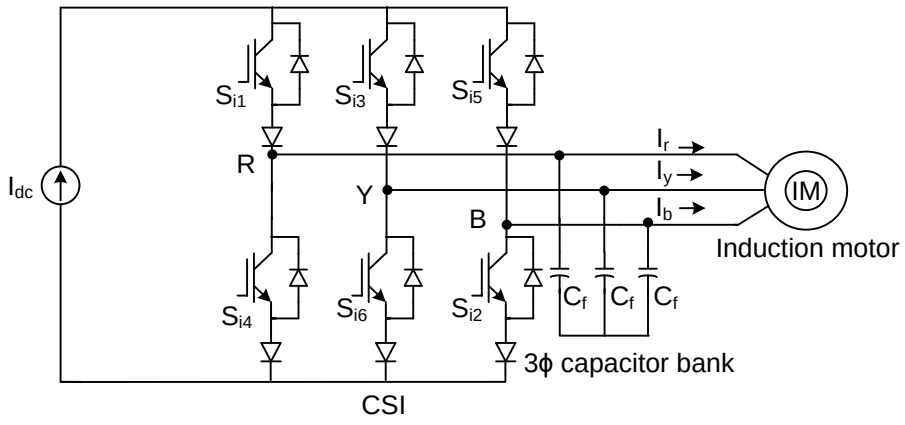

Figure 1.1: Basic structure of PWM IGBT CSI

A 0.75kW PWM CSI fed induction motor drive has been developed. The controlled current source required for the CSI drive shown in figure 1.1 can be realized with a simple SCR based controlled rectifier with a large series inductor. This configuration ensured bi-directional current flow. To minimize the size of the dc link inductor, to improve the dynamic performance of the drive and input power quality, it is recommended to use a PWM current source rectifier instead of three-phase SCR based controlled rectifier. In this project, the current source rectifier is replaced by a three-phase SCR converter. The DC link current is controlled by controlling the firing angle of three phase SCR converter.

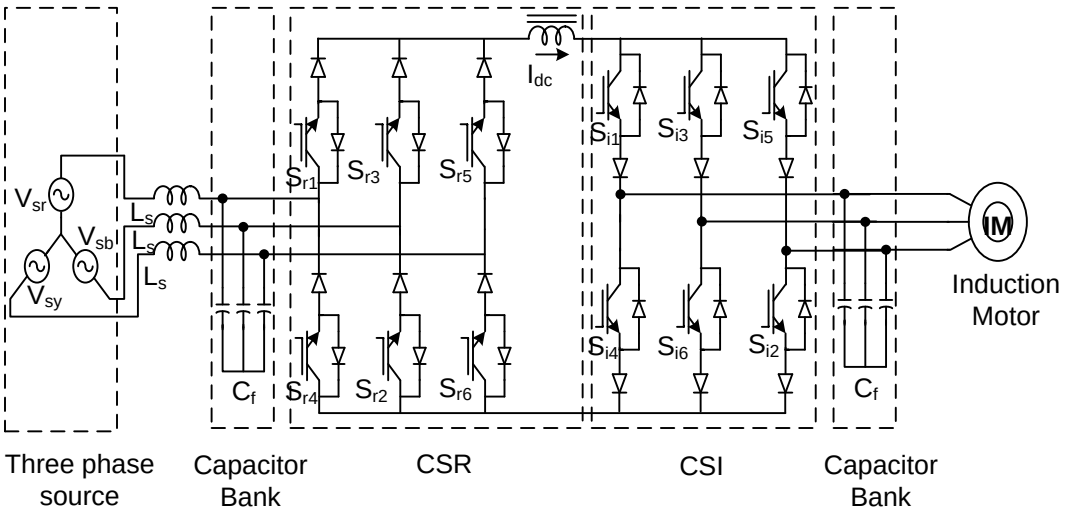

Figure 1.2: Power structure of CSI fed induction motor drive with CSR

1.3 Objective of the project

The objective of the project is to develop a PWM CSI fed sensorless vector controlled induction motor drive. A 0.75 kW induction motor is chosen for this purpose. The DC link current is derived from a thyristor controlled rectifier. The sensorless control is adopted from stator voltage model of an induction machine. Space vector modulation technique is adopted to generate pulse width modulated current. The control technique is implemented in TMS320F28335 DSP processor.

1.4 Organization of Thesis

Chapter 2 deals with the mathematical modeling of induction machine, sensorless vector control technique adopted for the PWM CSI fed drive.

Chapter 3 deals with the hardware design of PWM CSI fed induction motor drive. The basic features of Texas Instruments digital signal micro-controller TMS320F28335 are discussed. Analog signal conditioning board, protection board which acts as bridge between micro-controller and hardware are also discussed in this chapter.

Chapter 4 presents the simulation and hardware results with necessary explanations.

Chapter 5 presents the summary of the project work and future scope of the project.

CHAPTER 2

SENSORLESS FIELD ORIENTED CONTROL OF INDUCTION MOTOR AND SPACE VECTOR PWM

2.1 Introduction

This chapter gives the theoretical background for sensorless field oriented control of induction motor, design of controllers such as DC link current controller, flux controller and speed controller.

The objectives of the project are as follows,

- Detailed description of field oriented control (FOC) adopted for PWM-CSI fed induction motor drive.
- Sensorless FOC technique has been employed because the drive motor lies on the sea bed and sensored control requires laying of optic fibre all the way from sea surface to sea bed which results in enormous increase in installation cost and also causes delay in operation. In sensorless FOC, Motor speed can be estimated by estimating the rotor flux position.
- PWM CSI fed drive feeds sinusoidal currents and sinusoidal voltages to motor, which enhances the performance of the motor.
- PWM CSI fed drive has been implemented by employing following modulation techniques,

    1. Quasi square wave pulse width modulation technique by maintaining constant modulation index and varying DC link current.

    2. Space vector pulse width modulation technique by maintaining constant modulation index and varying DC link current.

    3. Space vector pulse width modulation technique by varying modulation index and maintaining constant DC link current.

- Complete closed loop control of CSI fed Induction motor drive is established by employing space vector pulse width modulation and varying dc link current while maintaining modulation index constant.

The following sections give a detailed description of space phasor, field oriented control technique for controlling induction motor, design of controllers and design of filter. This chapter also includes sensorless control algorithm, space vector pulse width modulation technique and their implementations.

2.2 Space Phasor

The traditional single phase equivalent circuit is best suited for sinusoidal quantities in steady state but not in transient state conditions. Therefore, the space vector theory has been developed for dealing with the transients in electrical machines.

The following assumptions have been made for space vector theory,

1. Air gap flux distribution is assumed to be sinusoidal,
2. Non-linearities are absent,
3. No iron losses and
4. Resistances and inductances are assumed to be independent of temperature and frequency.

The space phasor representation of stator RYB phase axes and stationary $\alpha\beta$ axes are shown in figure 2.1.

When three phase currents displaced by a space angle of 120^0 are fed to the three

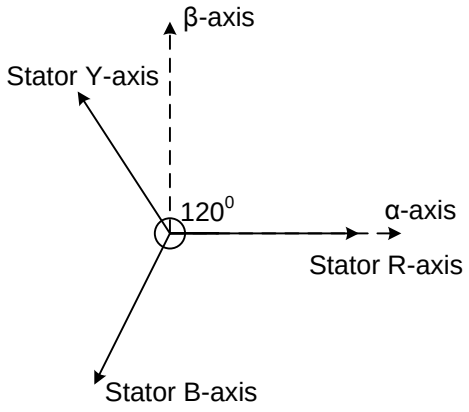

Figure 2.1: Space Phasor of RYB axes and $\alpha\beta$ axes

phase windings of induction motor, the resultant current space phasor has a magnitude of 1.5 times the peak value of phase current and the current space phasor rotates with synchronous speed in anti-clockwise direction.

The space vector notation of current phasor is described in equation 2.1.

$$\vec{i_s} = i_{sr} + i_{sy}e^{j\frac{2\pi}{3}} + i_{sb}e^{j\frac{4\pi}{3}} \tag{2.1}$$

The mathematical representation of three phase stator currents of induction motor are as follows,

$$i_{sr} = I_m sin(\omega_s t)$$

$$i_{sr} = I_m sin(\omega_s t - \frac{2\pi}{3})$$

$$i_{sr} = I_m sin(\omega_s t + \frac{2\pi}{3}) \tag{2.2}$$

Substituting three phase stator currents of induction machine in equation 2.1 gives the resultant current space phasor. Equation 2.3 represents the current space phasor has constant magnitude of 1.5 times the peak value of phase current and rotating with synchronous speed in anti-clockwise direction.

$$\vec{i_s} = \frac{3}{2}|I_m|e^{j\omega_s t} \tag{2.3}$$

On decomposing equation 2.1 into real and imaginary parts, the stationary α axis and β axis components of the three phase currents can be found. The α, β components of stator current phasor are given in equation 2.4 and equation 2.5.

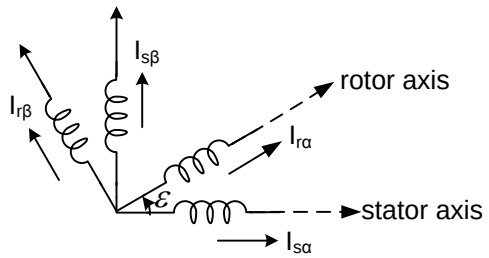

Figure 2.2: Equivalent coils of stator and rotor of induction motor

$$i_{s\alpha} = i_{sr} - \frac{i_{sy}}{2} - \frac{i_{sb}}{2} \tag{2.4}$$

$$i_{s\beta} = \frac{\sqrt{3}}{2}(i_{sy} - i_{sb}) \tag{2.5}$$

where,

i_{sr} is R-phase component of stator current

i_{sy} is Y-phase component of stator current

i_{sb} is B-phase component of stator current

$i_{s\alpha}$ is α-axis component of stator current

$i_{s\beta}$ is β-axis component of stator current

2.3 Field Oriented Control of Induction Motor

2.3.1 Stator and rotor flux distribution

The three phase currents displaced by 120^0 are fed to the stator windings of induction motor. As the stator windings of induction motor and currents are displaced by 120^0, the resultant magnetic field rotates at synchronous speed. Therefore, the stator poles are rotating at synchronous speed. Figure 2.3 represents the stationary R-phase axis, rotor R-pahse axis. Point A in the figure 2.3 represents a stationary point on the stator surface where the resultant MMF's are calculated. Point A is θ degree away from the stator R-phase axis. rotor R-pase axis is ϵ degree away from stator R-phase axis. Point A is β degree ahead from rotor R-phase axis.

Therefore, the stator Magnetomotive Force (MMF)(F_s) distribution is given as

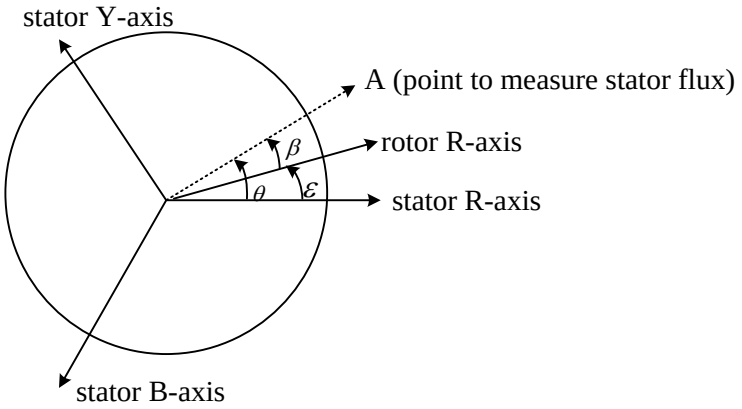

Figure 2.3: Rotating magnetic field

$$F_s = N_{se}I_{sr}(t)cos\theta + N_{se}I_{sy}(t)cos(\theta - 120^0) + N_{se}I_{sb}(t)cos(\theta + 120^0) \qquad (2.6)$$

$$F_s = \frac{N_{se}}{2}[e^{-j\theta}(i_{sr}(t)+i_{sy}(t)e^{j\frac{2\pi}{3}}+i_{sb}(t)e^{j\frac{4\pi}{3}})+e^{j\theta}(i_{sr}(t)+i_{sy}(t)e^{-j\frac{2\pi}{3}}+i_{sb}(t)e^{-j\frac{4\pi}{3}})] \tag{2.7}$$

$$F_s = \frac{N_{se}}{2}[e^{-j\theta}\overrightarrow{i_s(t)} + e^{j\theta}\overrightarrow{i_s^*(t)}] \tag{2.8}$$

where,

N_{se} is equivalent number of turns of stator

$\overrightarrow{i_s}$ is space vector of stator current

$\overrightarrow{i_s^*}$ is conjugate space vector of stator current

Similarly, resultant MMF (F_r) at point A due to current flowing in three-phase rotor circuit has been calculated. The rotor carries three phase currents and produces synchronously rotating magnetic field. The rotor MMF distribution is given as,

$$F_r = N_{re}I_{rr}(t)cos\beta + N_{re}I_{ry}(t)cos(\beta - 120^0) + N_{re}I_{rb}(t)cos(\beta + 120^0) \tag{2.9}$$

$$F_r = \frac{N_{re}}{2}[e^{-j\beta}(i_{rr}(t)+i_{ry}(t)e^{j\frac{2\pi}{3}}+i_{rb}(t)e^{j\frac{4\pi}{3}})+e^{j\theta}(i_{rr}(t)+i_{ry}(t)e^{-j\frac{2\pi}{3}}+i_{rb}(t)e^{-j\frac{4\pi}{3}})] \tag{2.10}$$

$$F_r = \frac{N_{re}}{2}[e^{-j\beta}\overrightarrow{i_r(t)} + e^{j\beta}\overrightarrow{i_r^*(t)}] \tag{2.11}$$

where,

N_{re} is equivalent number of turns of rotor

$\overrightarrow{i_r}$ is space vector of rotor current

$\overrightarrow{i_r^*}$ is conjugate space vector of rotor current

2.3.2 Stator and Rotor voltage equations

Stator flux and rotor flux space vector can be found out dividing the stator and rotor MMF space vectors by air gap reluctance. As an induction machine is a smooth air gap machine the stator and rotor flux space vector have same orientation that of stator

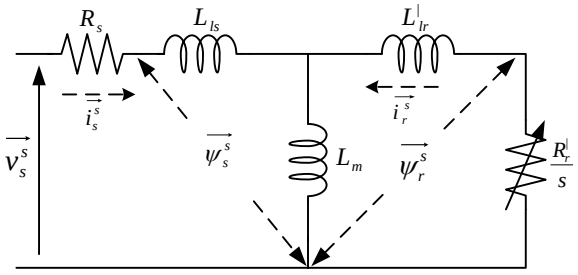

Figure 2.4: Per phase equivalent circuit of induction motor

MMF and rotor MMF respectively but scaled down by air gap reluctance. The stator voltage space vectors can be found out by addition of resistance drop space vector and time derivative of stator flux space vector. The rotor voltage space vector can also be found out in similar way. Figure 2.4 pictorially depicts the stator and rotor voltage space vectors. The stator and rotor voltage equations for squirrel cage induction motor are as follows,

$$\vec{v_s^s} = R_s \vec{i_s^s} + \frac{d\vec{\psi_s^s}}{dt} \tag{2.12}$$

$$0 = R_r \vec{i_r^r} + \frac{d\vec{\psi_r^r}}{dt} \tag{2.13}$$

where,

$\vec{v_s^s}$ is stator voltage per phase in stator reference frame

$\vec{i_s^s}$ is stator current per phase in stator reference frame

R_s is stator resistance per phase

$\vec{\psi_s^s}$ is stator flux linkage per phase in stator reference frame

$\vec{i_r^r}$ is rotor current per phase in rotor reference frame

R_r is rotor resistance per phase

$\vec{\psi_r^r}$ is rotor flux linkage per phase in rotor reference frame

The stator and rotor flux linkages in stator and rotor reference frames respectively are given as,

$$\vec{\psi_s^s} = L_s \vec{i_s^s} + L_m \vec{i_r^r} e^{j\epsilon} \tag{2.14}$$

$$\vec{\psi_r^r} = L_m \vec{i_s^s} e^{-j\epsilon} + L_r \vec{i_r^r} \tag{2.15}$$

where,

L_s is stator inductance per phase

L_m is mutual inductance per phase

L_r is rotor inductance per phase

L_{ls} is stator leakage inductance per phase

L_{lr} is rotor leakage inductance per phase

The mathematical expression for voltage space phasor is given in equation 2.16.

$$\vec{v_s^s} = \frac{3}{2} V_m e^{j\omega_s t} \tag{2.16}$$

similarly, the stator and rotor current space phasors are defined as,

$$\vec{i_s^s} = \frac{3}{2} I_{ms} e^{j\omega_s t} \tag{2.17}$$

$$\vec{i_r^r} = \frac{3}{2} I_{mr} e^{j(\omega_s - \omega)t} \tag{2.18}$$

The stator current space phasor rotates at synchronous speed (ω_s) with respect to stator and has a constant magnitude of 1.5 times peak value of stator phase current. The rotor current space phasor rotates at slip speed (ω_{slip}) with respect to rotor and has a magnitude of 1.5 times peak value of rotor phase current. where,

I_{ms} is the peak value of stator per phase current

I_{mr} is the peak value of rotor per phase current

ω_s is the synchronous speed in rad/sec

ω is the actual speed of motor in rad/sec

The phasor diagram of induction motor using stator voltage equation (equation 2.12), rotor voltage equation (equation 2.13), stator flux linkage equation (equation 2.14) and rotor flux linkage equation (equation 2.15) is shown in figure 2.5. Rotor flux linkage in stator reference frame is given as,

$$\vec{\Psi_r^s} = L_m \vec{i_{mr}^s} \tag{2.19}$$

$\vec{i_{mr}^s}$ is the rotor magnetizing current in stator flux reference frame. Figure 2.6 represents the relation between the rotor axis and rotor flux axis. Rotor flux axis rotates at synchronous speed whereas rotor axis rotates at electrical speed of induction motor.

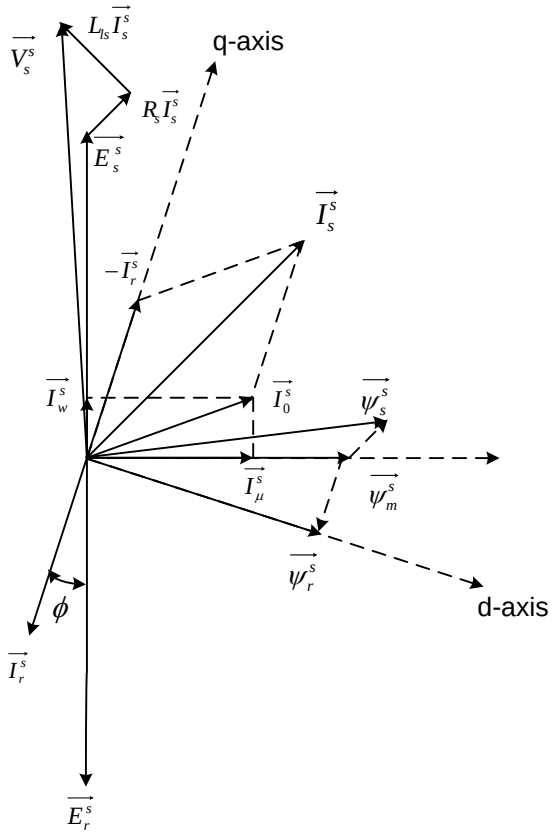

Figure 2.5: Phasor diagram of induction motor

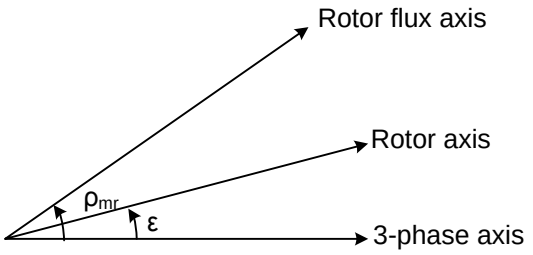

Figure 2.6: Rotor and rotor flux axis of induction motor

$$L_m\overrightarrow{i_{mr}^s} = L_m\vec{i}_s^s + L_r\vec{i}_r^r e^{j\epsilon} \tag{2.20}$$

$$L_m\overrightarrow{i_{mr}^s} = L_m(\vec{i}_s^s + \vec{i}_r^r e^{j\epsilon}) + L_{lr}\vec{i}_r^r e^{j\epsilon} \tag{2.21}$$

$$\vec{i}_r^r = \frac{1}{1+\sigma_r}(\overrightarrow{i_{mr}^s} - \vec{i}_s^s)e^{-j\epsilon} \tag{2.22}$$

where,

$$\sigma_r = \frac{L_{lr}}{L_m} \tag{2.23}$$

L_{lr} is per phase leakage reactance of rotor

Equation (2.24) can be written from equation 2.15,

$$R_r \vec{i_r^r} + L_r \frac{d\vec{i_r^r}}{dt} + L_m \frac{d}{dt}(\vec{i_s^s} e^{-j\epsilon}) = 0 \tag{2.24}$$

substituting equation 2.22 in equation 2.24, and transforming the equation to rotor flux reference frame, equations (2.25) - (2.28) are obtained.

$$\frac{R_r}{1+\sigma_r} i_{mr} - \frac{R_r}{1+\sigma_r} i_{sd} + L_m \frac{di_{mr}}{dt} = 0 \tag{2.25}$$

which implies,

$$i_{sd} = i_{mr} + T_r \frac{di_{mr}}{dt} \tag{2.26}$$

$$-\frac{R_r}{1+\sigma_r} i_{sq} - L_m \omega_e i_{mr} + L_m \omega_{mr} i_{mr} = 0 \tag{2.27}$$

which implies,

$$\omega_{slip} = \frac{i_{sq}}{T_r i_{mr}} \tag{2.28}$$

Developed torque in an induction machine can be written as

$$m_d = \frac{2}{3}\frac{P}{2} L_m Imag(\vec{i_s^s}(\vec{i_r^r} e^{j\epsilon})^*) \tag{2.29}$$

Substituting Equation 2.22 in Equation 2.29 results in

$$m_d = \frac{2}{3}\frac{P}{2}\frac{L_m}{1+\sigma_r} i_{sq} i_{mr} \tag{2.30}$$

where,

P is number of poles

$T_r = \frac{L_r}{R_r}$ is rotor time constant of induction motor

ω_e is electrical speed of induction motor in rad/sec

The dynamic equation of the machine can be written as,

$$m_d - m_l = J\frac{d\omega}{dt} + B\omega \tag{2.31}$$

where,

ω is mechanical speed of induction motor in rad/sec

m_d is torque developed by motor

m_l is load torque on motor

J is moment of inertia of motor

B is frictional co-efficient

From equation 2.26, it is clear that the rotor magnetizing current (i_{mr}) depends on direct axis component of stator current (i_{sd}). Therefore, the rotor magnetizing current can be controlled by controlling i_{sd}. From equation 2.30, torque developed depends on quadrature axis component of stator current i_{sq} and rotor magnetizing current i_{mr}. As i_{mr} can be controlled by i_{sd}, the torque developed by induction motor can be controlled independently by controlling i_{sq}. Therefore, by employing FOC technique of induction motor, decoupled control of flux and torque can be achieved.

2.4 Sensorless control algorithm

Generally a speed sensor such as incremental encoder is mounted on the shaft of the motor to measure the speed of the motor which is required for closed loop control. In sensorless operation, the speed signal is estimated using stator voltage and current signals. It is important to estimate the rotor flux position for vector controlled drive. The rotor flux position is also estimated using the stator voltage and current information. The sensorless technique can be implemented in several ways. One of the simple and popular technique is indirect estimation of speed from estimation of rotor flux position vector. In this method the rotor flux is first estimated from stator voltage and current. After estimating the rotor flux position, the synchronous speed of induction motor is determined by differentiating the rotor flux position. The actual speed of motor can be determined by subtracting slip speed from synchronous speed. This estimated speed is used for the vector control drive.

The sensorless control algorithm adopted in this report is elaborated below.,

From stator voltage equation of induction motor i.e., equation 2.12,

$$\vec{\psi_s^s} = \int (\vec{v_s^s} - R_s \vec{i_s^s}) dt \tag{2.32}$$

The stator and rotor flux linkages in stator flux reference frame are as follows,

$$\vec{\psi_s^s} = L_s \vec{i_s^s} + L_m \vec{i_r^s} \tag{2.33}$$

$$\vec{\psi_r^s} = L_m \vec{i_s^s} + L_r \vec{i_r^s} \tag{2.34}$$

From equation 2.33, rotor current in stator flux reference frame can be written as,

$$\vec{i_r^s} = \frac{\vec{\psi_s^s} - L_s \vec{i_s^s}}{L_m} \tag{2.35}$$

Rotor flux linkage space vector referred in stator reference frame can be obtained by substituting rotor current in stator flux reference frame ($\vec{i_r^s}$) obtained from equation 2.35 in rotor flux linkage in stator reference frame equation 2.34,

$$\vec{\psi_r^s} = \frac{L_r}{L_m} \vec{\psi_s^s} - \frac{L_s L_r - L_m^2}{L_m} \vec{i_s^s} \tag{2.36}$$

Decomposing equation 2.36 into $\alpha\beta$ components results in stationary α axis component of rotor flux ($\psi_{r\alpha}^s$) and β axis component of rotor flux ($\psi_{r\beta}^s$) and are as follows,

$$\psi_{r\alpha} = \frac{L_r}{L_m} \psi_{s\alpha} - \frac{L_s L_r - L_m^2}{L_m} i_{s\alpha} \tag{2.37}$$

$$\psi_{r\beta} = \frac{L_r}{L_m} \psi_{s\beta} - \frac{L_s L_r - L_m^2}{L_m} i_{s\beta} \tag{2.38}$$

Therefore, the rotor flux position (ρ_{mr}) can be estimated using stator voltages, stator currents and machine parameters. The rotor flux position (ρ_{mr}) can be mathematically calculated using equations 2.37 and 2.38 as,

$$\rho_{mr} = Tan^{-1}(\frac{\psi_{r\beta}}{\psi_{r\alpha}}) \tag{2.39}$$

The block diagram of sensorless operation for estimating the rotor flux position and

speed is shown in figure 2.7.

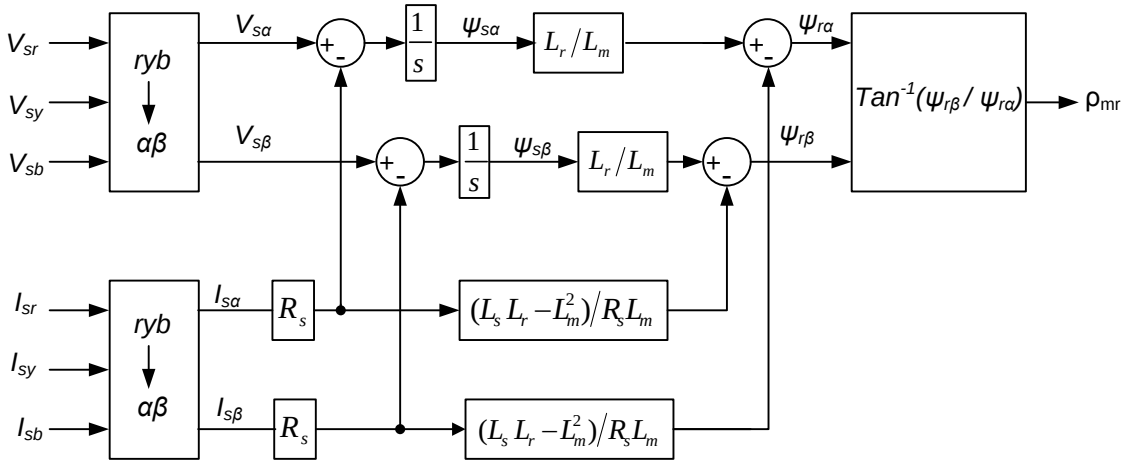

Figure 2.7: Block diagram of sensorless operation

In sensorless operation of estimating flux, the pure integrator is replaced by an integrator with small amount of negative feedback.Employing pure integrator may result in various errors such as measurement noise, parameter de-tuning and input dc offsets. Negative feedback is to stabilise the integrator output against the errors especially dc offset. The modified integrator is shown in figure 2.8.

After estimating the rotor flux position (ρ_{mr}), the synchronous speed of induction mo-

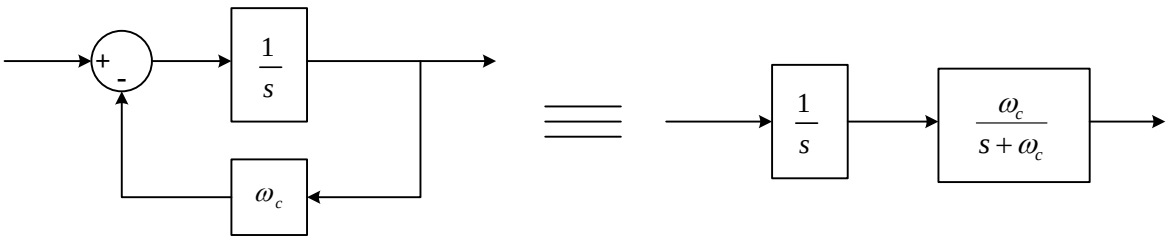

Figure 2.8: Modified integrator with feedback

tor can be estimated by differentiating ρ_{mr} with respect to time. So as to avoid inverse tan operation, it is recommended to estimate the synchronous speed of motor using $cos\rho_{mr}$ and $sin\rho_{mr}$. The mathematical approach for estimating the synchronous speed (ω_{mr}) is as follows,

$$\omega_{mr} = \frac{d\rho_{mr}}{dt}$$

$$\omega_{mr} = \frac{d\rho_{mr}}{dt}(cos^2\rho_{mr} + sin^2\rho_{mr})$$

$$\omega_{mr} = cos\rho_{mr}\frac{dsin\rho_{mr}}{dt} - sin\rho_{mr}\frac{dcos\rho_{mr}}{dt} \tag{2.40}$$

The following block diagram represents the estimation of synchronous speed from $cos\rho_{mr}$ and $sin\rho_{mr}$.

Therefore, the speed of induction motor can be calculated by subtracting slip speed

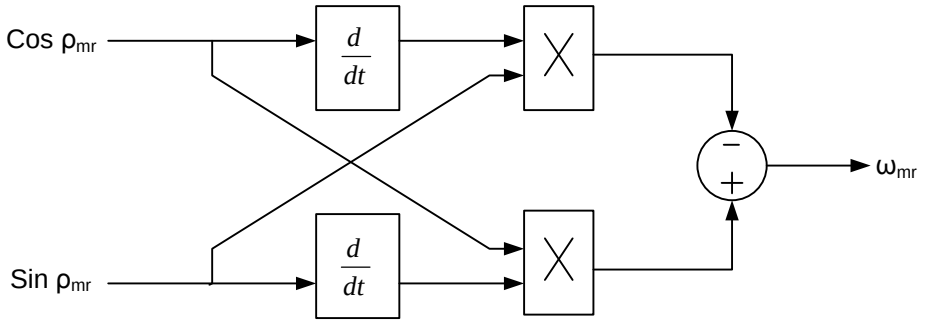

Figure 2.9: Block diagram for estimating ω_{mr} from $cos\rho_{mr}$ and $sin\rho_{mr}$

(ω_{slip}) from synchronous speed (ω_{mr}) as in equation 2.41.

$$\omega = \omega_{mr} - \frac{i_{sq}}{T_r i_{mr}} \tag{2.41}$$

From equation 2.28, slip speed of induction motor is defined as,

$$\omega_{slip} = \frac{i_{sq}}{T_r i_{mr}}$$

2.5 Power structure of CSI fed induction motor drive with 3ϕ SCR converter

The power structure of CSI fed induction motor drive comprises of 3ϕ SCR converter, a heavy series inductor, current source inverter and a 3ϕ induction motor. The 3ϕ SCR converter is fed from 3ϕ source and it converts alternating voltage to controlled DC voltage. The heavy series inductor at the output of the SCR converter converts controlled DC voltage to controlled DC current. The DC link current is controlled by controlling the firing angle of SCR converter. This controlled current is fed to current source inverter and inverter converts controlled current to alternating current. This alternating current is fed to induction motor. The PWM technique employed is space vector pulse width modulation.The control algorithms for the drive has been implemented on digital

platform using digital signal controller (DSC) TMS320F28335. A 3ϕ capacitor bank has been installed at the output of the inverter which assists in commutation and in filtering of harmonics. The complete power structure of the CSI fed induction motor drive with 3ϕ SCR converter is shown in figure 2.10.

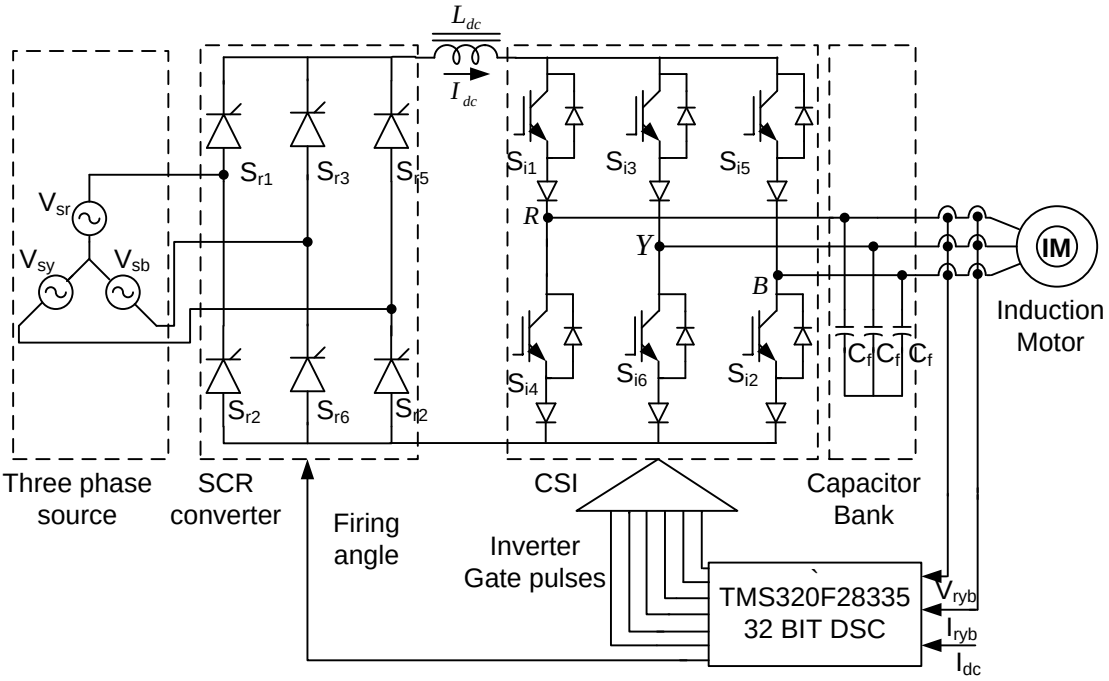

Figure 2.10: Power structure of CSI fed induction motor drive with 3ϕ SCR converter

The CSI fed Induction motor drive is implemented by the following techniques,

• Quasi square wave PWM technique and varying DC link current by maintaining constant modulation index.

• Space vector PWM technique and varying DC link current by maintaining constant modulation index.

• Space vector PWM technique and varying modulation index by maintaining constant DC link current.

The complete simulation and hardware results for CSI fed Induction motor drive have been presented in Chapter 4 by employing Space Vector PWM technique and varying DC link current all the while maintaining constant modulation index. The 3ϕ SCR converter can be replaced by a PWM current source rectifier (CSR), which provides constant DC current with low total harmonic distortion (THD), superior dynamic

response and more reliable output compared with 3ϕ SCR converter.

2.6 Control algorithms for CSI fed induction motor drive

The block diagram for induction motor model used for CSI drive is shown in figure 2.11. DC link current (I_{dc}) controller, direct axis component of stator current (I_{sd}) controller for controlling flux and quadrature axis component of stator current (I_{sq}) controller for controlling torque have been employed in CSI fed induction motor drive.

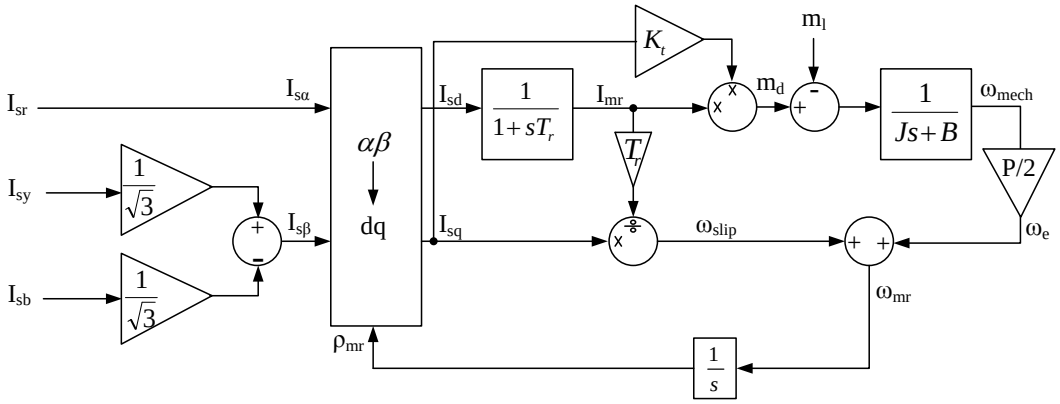

Figure 2.11: Induction motor model used for CSI drive

The block diagram of complete CSI fed FOC of induction motor is shown in figure 2.12. The output of flux controller is reference value of direct axis component of stator current. The output of speed controller is reference value of quadrature axis component of stator current. The reference values of direct axis and quadrature axis components of stator current results in generation of reference value of DC link current. When the reference values of direct axis and quadrature axis components are divided by reference value of DC link current, converting the resultant dq components to 3ϕ components results in 3ϕ unit vectors. These unit vectors are used for generation of gating pulses for inverter.

The output of DC link current controller is rectifier voltage. When this rectifier voltage is divided with maximum gain of converter, cosine of firing angle of SCR converter is generated, resulting in generation of gating pulses for 3ϕ SCR converter.

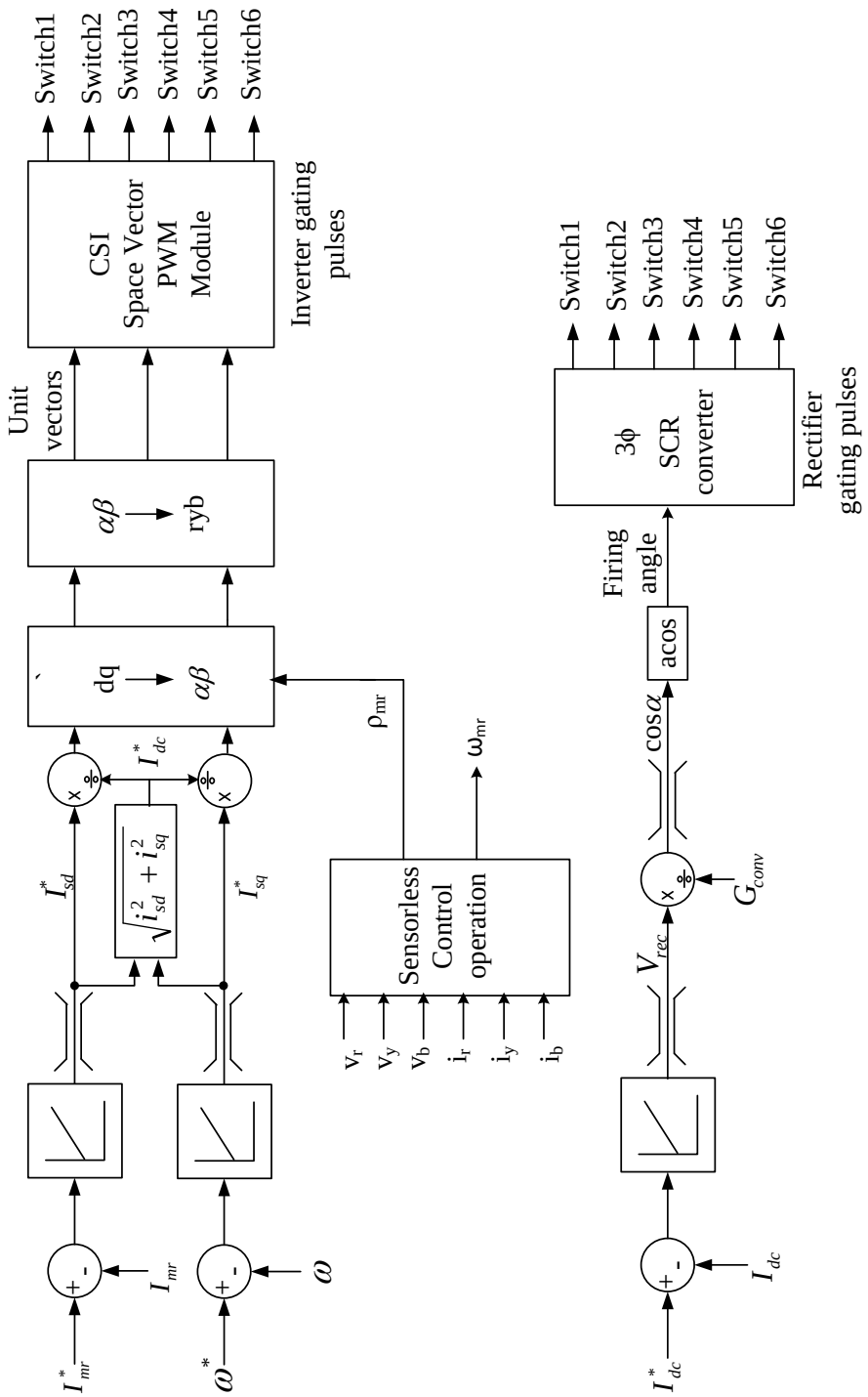

Figure 2.12: Block diagram of complete control structure of CSI fed induction motor drive

2.6.1 PI Controller

PI controller is a combination of proportional term (K_p) and an integral (K_i) term. The transfer function of PI controller can be mathematically defined as,

$$Transfer\ function\ of\ PI\ controller = K_p + \frac{K_i}{s} \tag{2.42}$$

PI controller can also be implemented as,

$$Transfer\ function\ of\ PI\ controller = K_{pi}(\frac{1 + sT_{pi}}{sT_{pi}}) \tag{2.43}$$

When a PI controller is implemented in the plant control system, PI controller increases the speed of response and eliminates the steady state error. The error signal E(s) is generated from the difference of reference signal R(s) and actual output signal C(s) and is fed to PI controller. PI controller generates appropriate control signal and is fed for achieving desired output. Figure 2.13 elaborates a PI controller connected with the plant.

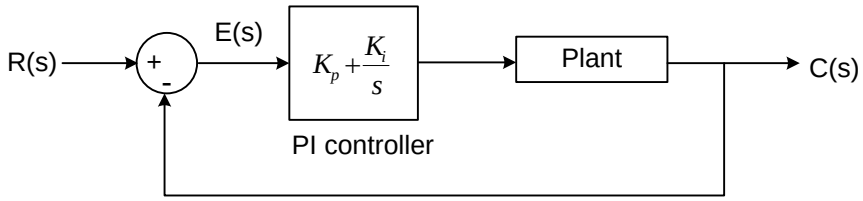

Figure 2.13: Implementation of PI controller

2.6.2 Flux controller

Flux in induction motor can be controlled by rotor magnetizing current (i_{mr}) which in turn solely depends on direct axis component of stator current (i_{sd}). The mathematical relation between i_{mr} and i_{sd} is given in equation 2.26.

$$i_{sd} = i_{mr} + T_r \frac{di_{mr}}{dt}$$

The above equation can be represented in the form of block diagram as shown in

figure 2.14.

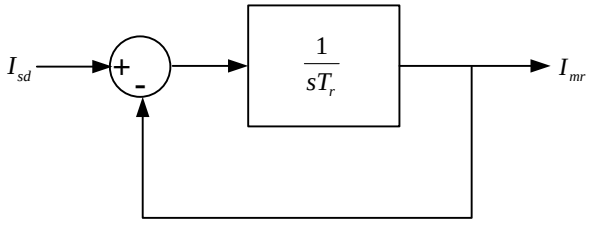

Figure 2.14: Block diagram representing relation between i_{mr} and i_{sd}

The transfer function of the block diagram shown above can be written as,

$$I_{sd}(s) = \frac{1}{1 + sT_r} I_{mr}(s) \tag{2.44}$$

The difference of reference rotor magnetizing current and actual magnetizing current is fed to flux controller. The flux controller output is i_{sd} reference. Figure 2.15 represents the above statement.

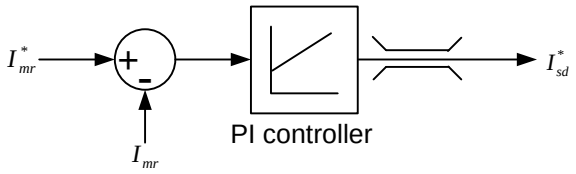

Figure 2.15: Flux controller

The block diagram of flux controller is shown in figure 2.16. In which, the reference value of magnetizing current (i^*_{mr}) can be determined by using the ratings of machine and machine parameters. The actual rotor magnetizing current i_{mr} can be determined by using equation 2.26. The error signal is fed to PI controller for necessary control action.

The transfer function of PI controller is considered as given in equation 2.43. The

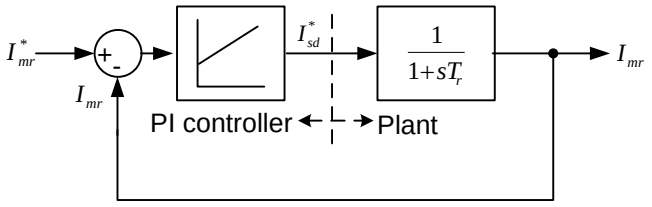

Figure 2.16: Block diagram of flux controller

system shown in figure 2.16 is assumed as a first order system shown in figure 2.17 and

assuming appropriate bandwidth, the parameters K_{pi} and T_{pi} are determined.

where,

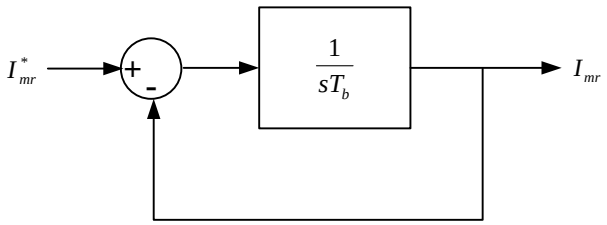

Figure 2.17: Block diagram of first order system

T_b is the assumed bandwidth of the system.

The parameters of flux controller are defined as,

$$T_{pi} = T_r \tag{2.45}$$

$$K_{pi} = \frac{T_{pi}}{T_b} \tag{2.46}$$

2.6.3 Speed controller

Speed of the induction motor depends on torque developed by the motor which in turn depends on quadrature axis component of stator current (i_{sq}) and rotor magnetizing current (i_{mr}) as in equation 2.47.

$$m_d \propto i_{sq} i_{mr} \tag{2.47}$$

As i_{mr} is controlled by i_{sd}, the torque developed by the motor can be independently controlled by i_{sq}. The difference of reference speed and actual speed is fed to speed controller. The speed controller gives quadrature component of stator current (i_{sq}) as output. Figure 2.18 represents the above statement.

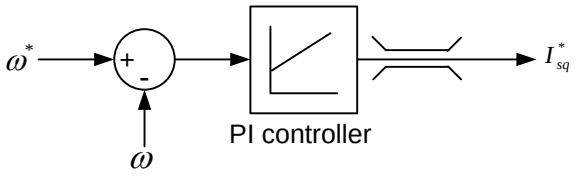

Figure 2.18: Speed controller

Figure 2.19 represents the block diagram of speed controller. Similarly, as in Flux controller, the system as assumed as first order system with appropriate bandwidth. Then the parameters of the PI controller are defined as in equations 2.48 and 2.49.

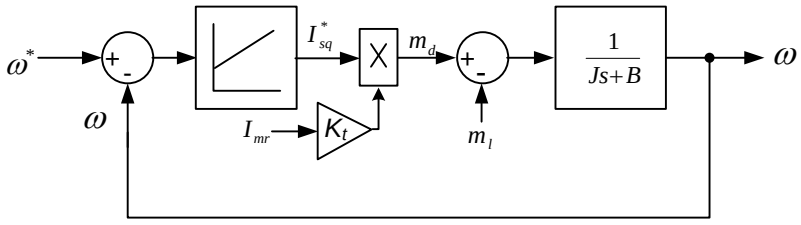

Figure 2.19: Block diagram of speed controller

$$T_{pi} = \frac{J}{B} \tag{2.48}$$

$$K_{pi} = \frac{J}{T_b} \tag{2.49}$$

2.6.4 DC link current controller

DC link current can be controlled by controlling the firing angle of 3ϕ SCR converter. Considering there is no delay in plant, the parameters of the PI controller are determined. The DC link current controller output is rectifier voltage. When this rectifier voltage is divided by maximum gain of the converter (G_{Conv}), it results in cosine of firing angle of 3ϕ SCR converter. Figure 2.20 represents the above statement.

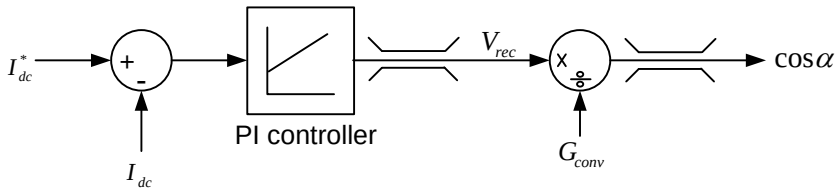

Figure 2.20: DC link current controller

The block diagram of DC link current controller is shown in figure 2.21. As done in earlier controllers, the parameters of DC link current controller are determined by assuming appropriate bandwidth. The parameters of DC link current controller are as follows,

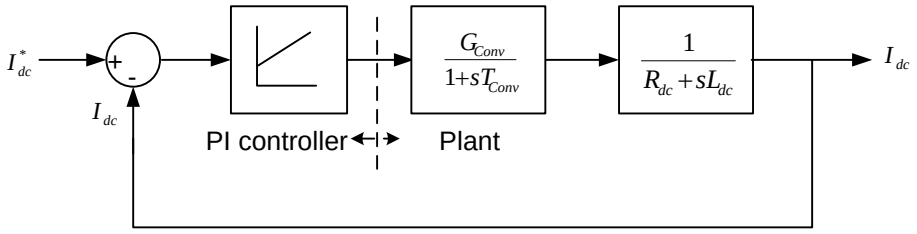

Figure 2.21: Block diagram of DC link current controller

$$T_{pi} = \frac{L_{dc}}{R_{dc}} \tag{2.50}$$

$$K_{pi} = \frac{L_{dc}}{T_b G_{Conv}} \tag{2.51}$$

where,

G_{Conv} is maximum gain of 3ϕ SCR converter

The generation of DC link current reference and generation of gating pulses for the inverter switches is shown in figure 2.22.

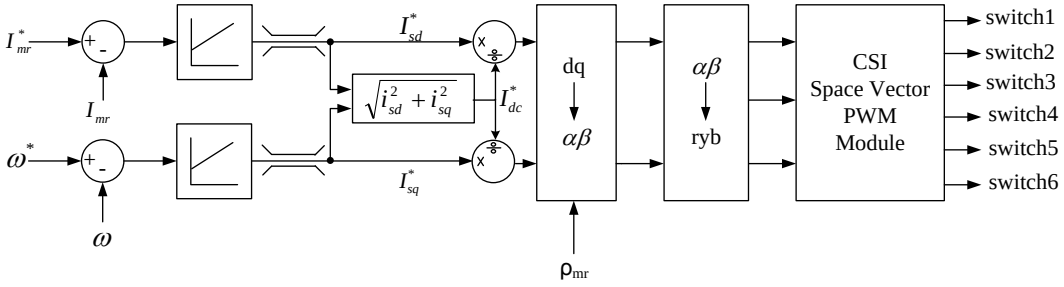

Figure 2.22: Block diagram for generation of DC link current reference and gating pulses for inverter switches

2.7 Space Vector Pulse Width Modulation

2.7.1 Switching states

In space vector PWM, at any instant only two switches of the inverter should conduct, one from the top commutation group and the other from the bottom commutation group.

Based on the constraint stated above, 9 switching states are possible from a two level CSI. Out of the 9 switching states [1], 6 switching states are called as active switching states and the other 3 are called as zero switching states.

In active switching states, two switches of different phases are conducted at any instant. Whereas, in zero switching states, two switches belonging to same phase conduct resulting in short circuit of the inverter leg. Table 2.1 represents the current space phasors, corresponding inverter switches to be turned ON and currents in 3 phases of inverter. $\vec{I_0}$ represents zero switching state while the other states $\vec{I_1}$ to $\vec{I_6}$ represents active switching states.

Switching state	Switches to be turned ON	Space Vector	$\vec{i_r}$	$\vec{i_y}$	$\vec{i_b}$
Zero switching state	(1, 4)	$\vec{I_0}$	0	0	0
	(2, 5)	$\vec{I_0}$	0	0	0
	(3, 6)	$\vec{I_0}$	0	0	0
Active switching state	(6, 1)	$\vec{I_1}$	I_{dc}	-I_{dc}	0
	(1, 2)	$\vec{I_2}$	I_{dc}	0	-I_{dc}
	(2, 3)	$\vec{I_3}$	0	I_{dc}	-I_{dc}
	(3, 4)	$\vec{I_4}$	-I_{dc}	I_{dc}	0
	(4, 5)	$\vec{I_5}$	-I_{dc}	0	I_{dc}
	(5, 6)	$\vec{I_6}$	0	-I_{dc}	I_{dc}

Table 2.1: Switching states and Space vectors in CSI SVPWM

2.7.2 Space Vector

The active vectors $\vec{I_1}$ to $\vec{I_6}$ form the regular hexagon with six equal sectors and zero vector $\vec{I_0}$ lies at the center of the hexagon. The relationship between the space vectors

and switching states can be found by assuming the system in balanced condition i.e.,

$$\vec{i_r} + \vec{i_y} + \vec{i_b} = 0 \tag{2.52}$$

Transforming the stator 3ϕ currents into stationary $\alpha\beta$ components using Clarke's transformation results in α and β components. Clarke's transformation is as follows,

$$i_{s\alpha} = \frac{2}{3} i_{sr} - \frac{1}{3} i_{sy} - \frac{1}{3} i_{sb} \tag{2.53}$$

$$i_{s\beta} = \frac{1}{\sqrt{3}} i_{sy} - \frac{1}{\sqrt{3}} i_{sb} \tag{2.54}$$

The space vector diagram of current source inverter is shown in figure 2.23 representing the positions of active vectors and zero vectors. The space vector notation of

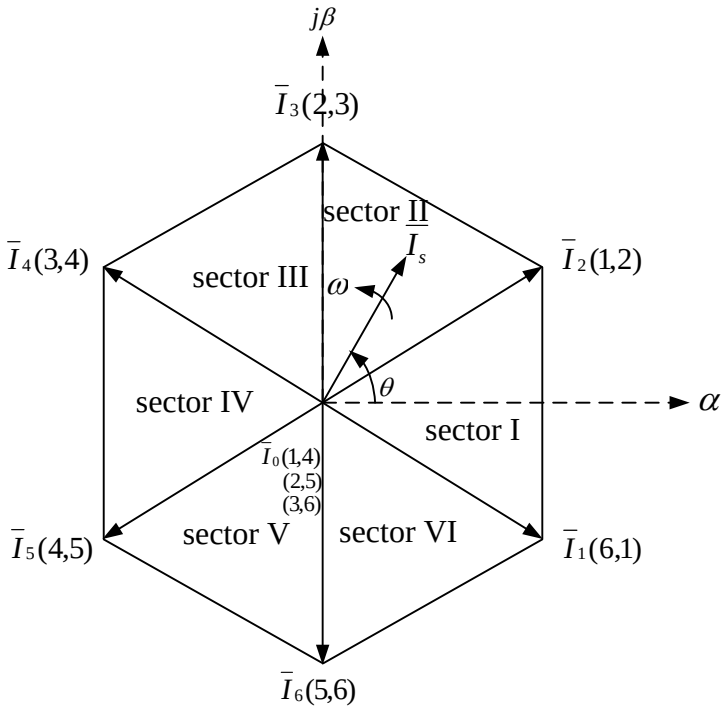

Figure 2.23: Space vector diagram for CSI

the current phasor is defined as,

$$\vec{i_s} = \frac{2}{3}(i_{sr} + i_{sy} e^{j\frac{2\pi}{3}} + i_{sb} e^{j\frac{4\pi}{3}}) \tag{2.55}$$

When the switches 6 and 1 of inverter are turned on. The current in R-phase of inverter is I_{dc} and the current in Y-phase of the inverter is $-I_{dc}$. This results in active switching

state $\vec{I_1}$.

$$\vec{I_1} = \frac{2}{\sqrt{3}} I_{dc} e^{\frac{-j\pi}{6}} \tag{2.56}$$

Similarly, the other five active vectors can also be derived. The generalized expression for active vectors is,

$$\vec{I_k} = \frac{2}{\sqrt{3}} I_{dc} e^{-j((k-1)\frac{\pi}{3} - \frac{\pi}{6})} \tag{2.57}$$

where, k is the sector number.

2.7.3 Dwell time calculation

Dwell time calculation is based on the Ampere-second balance, i.e., product of current space phasor ($\vec{I_s}$) and switching period (T_s) is equal to sum of the product of corresponding vectors and corresponding time intervals. i.e.,

$$\vec{I_s} T_s = \vec{I_1} T_1 + \vec{I_2} T_2 + \vec{I_0} T_0 \tag{2.58}$$

and

$$T_s = T_1 + T_2 + T_0 \tag{2.59}$$

The synthesis of the space phasor ($\vec{I_s}$) [1] from the corresponding active vectors and zero vectors is shown using the phasor diagram shown in figure 2.24.

On decomposing the current space phasor ($\vec{I_s}$) into $\alpha\beta$ components,

$$I_s cos(\theta) T_s = I_d (T_1 + T_2) \tag{2.60}$$

$$I_s sin(\theta) T_s = \frac{1}{\sqrt{(3)}} I_d (-T_1 + T_2) \tag{2.61}$$

Solving equations 2.60 and 2.61, dwell times T_1 and T_2 can be calculated, which implies that active vector $\vec{I_6}$ should be applied for T_1 duration and active vector $\vec{I_1}$ should be applied for T_2 duration with in a switching period (T_s).

$$T_1 = m_a sin(\frac{\pi}{6} - \theta) T_s \tag{2.62}$$

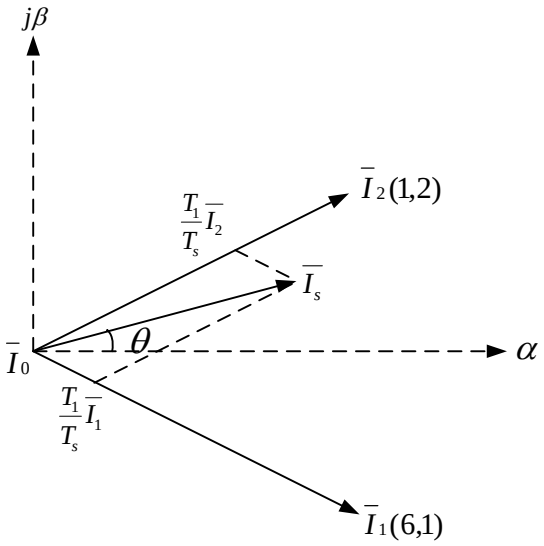

Figure 2.24: Synthesis of space vector using phasor

$$T_2 = m_a sin(\frac{\pi}{6} + \theta)T_s \tag{2.63}$$

Zero vector duration can be applied for T_0 which can be calculated using equation 2.64.

$$T_0 = T_s - T_1 - T_2 \tag{2.64}$$

where,

m_a is modulation index and is defined as,

$$m_a = \frac{I_s}{I_{dc}}; \qquad 0 \leq m_a \leq 1 \tag{2.65}$$

The generalized expressions for finding dwell times T_1 and T_2 can be found by replacing θ with $\theta^|$. where,

$$\theta^| = \theta - (k-1)\frac{\pi}{3}; \qquad -\frac{\pi}{6} \leq \theta^| \leq \frac{\pi}{6} \tag{2.66}$$

2.7.4 Switching sequence

In space vector PWM for CSI, the switching sequence should satisfy the following requirements for minimization of switching frequencies [1],

1. The transition from one switching state to another switching state should involve only two switches i.e., one switch being turned on and the other being turned off.

2. The transition of space vector from one sector to the other sector result in minimum

number of switches.

The switching sequence employed in space vector PWM of current source inverter, time periods for active vectors, zero vectors and corresponding switches to be turned ON for various sectors is described in Table 2.2. For example, if the current space phasor is in sector-II, then the active vectors of sector-II are $\vec{I_2}$ and $\vec{I_3}$ and zero vector is $\vec{I_0}$. Correspondingly, $\vec{I_2}$ should be turned ON for T_1 duration, $\vec{I_3}$ should be turned ON for T_2 duration and $\vec{I_0}$ should be turned ON for T_0 duration in a switching period (T_s).

In CSI fed drives, current should be continuous. If there is any discontinuity in current,

Sector	T_1	T_2	T_0
Sector I	$\vec{I_1}$ (1, 6)	$\vec{I_2}$ (1, 2)	$\vec{I_0}$ (1, 4)
Sector II	$\vec{I_2}$ (2, 1)	$\vec{I_3}$ (2, 3)	$\vec{I_0}$ (2, 5)
Sector III	$\vec{I_3}$ (3, 2)	$\vec{I_4}$ (3, 4)	$\vec{I_0}$ (3, 6)
Sector IV	$\vec{I_4}$ (4, 3)	$\vec{I_5}$ (4, 5)	$\vec{I_0}$ (4, 1)
Sector V	$\vec{I_5}$ (5, 4)	$\vec{I_6}$ (5, 6)	$\vec{I_0}$ (5, 2)
Sector VI	$\vec{I_6}$ (6, 5)	$\vec{I_1}$ (6, 1)	$\vec{I_0}$ (6, 3)

Table 2.2: Switching sequence for Space Vector PWM of CSI

high voltage appears across the switches resulting in damage of switches. Therefore for continuous flow of current, an overlapping period (μ) has been employed. During this period, the subsequent switch is turned-ON before the current switch is turned-OFF from the same commutation group.

Figure 2.25 represents the various switches to be turned ON for various durations T_1, T_2 and T_0 in a switching period (T_s) when the current space phasor (I_s) in sector-I and μ is overlapping angle during transition in switches.

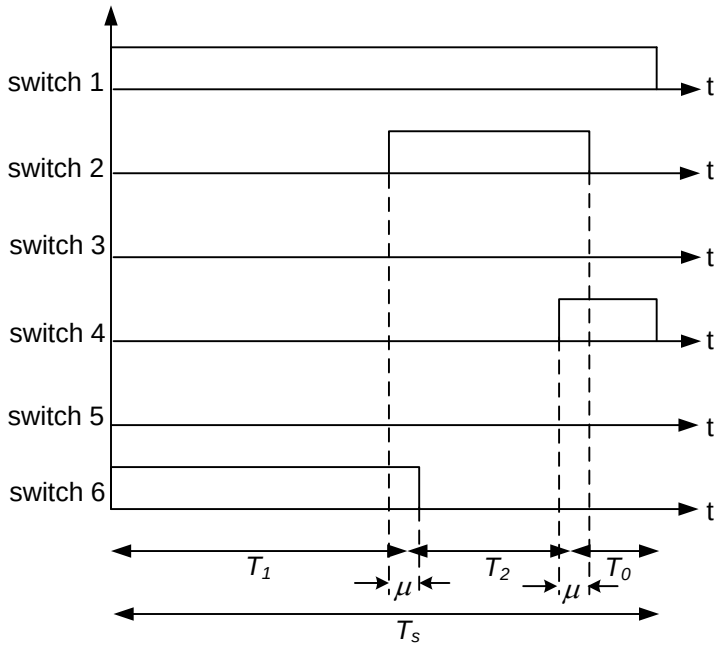

Figure 2.25: Switching sequence for I_s in sector-I

2.8 Design of Filter

Design of filter capacitor bank is one of the challenges in CSI fed induction motor drive. The per phase equivalent circuit for CSI fed induction motor drive is shown in figure 2.26.

At rated supply frequency (50Hz) and at no load, slip of the induction motor is approx-

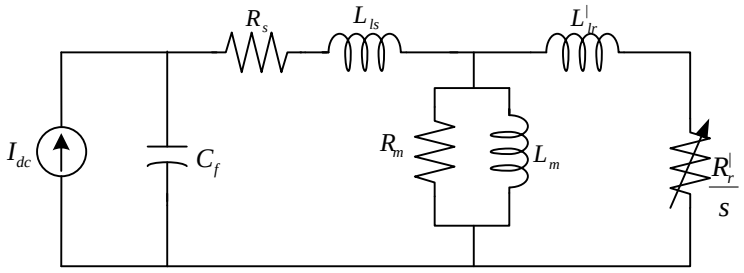

Figure 2.26: Equivalent circuit for CSI fed induction motor drive

imately equal to zero. Therefore, rotor resistance is very high compared to magnetizing inductance. Therefore rotor resistance branch can be treated as open. The equivalent circuit for the drive is shown in figure 2.27. During this instant, majority of current should flow through the magnetizing reactance compared to filter capacitor. At this operating frequency (50Hz), filter capacitance should be chosen such that reactance of filter capacitance is high compared to reactance of magnetizing current. Therefore, most of the fundamental current (frequency lesser than 50 Hz) flows through the ma-

chine magnetizing reactance.

The relation between filter capacitor current and magnetizing reactance current is given

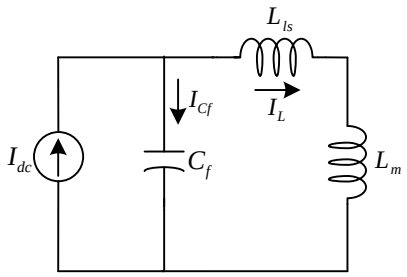

Figure 2.27: Equivalent circuit for CSI fed induction motor drive at normal operating frequencies

as,

$$\frac{I_{Cf}}{I_{Lm}} = \frac{X_{Lls} + X_{Lm}}{X_{Cf}} = [(L_{ls} + L_m)(C_f)]\omega_f^2 \tag{2.67}$$

where,

ω_f is normal operating frequency (50Hz)

At harmonic frequencies (5th,7th and onwards), slip of induction motor approximately equals one. During this instant, filter capacitance should be chosen such that majority current flows through rotor leakage reactance (L_{lr}) and rotor resistance (R_r) instead of magnetizing reactance (L_m). The equivalent circuit at harmonic frequencies is shown in figure 2.28. Neglecting stator and rotor resistances, the current through filter capacitor

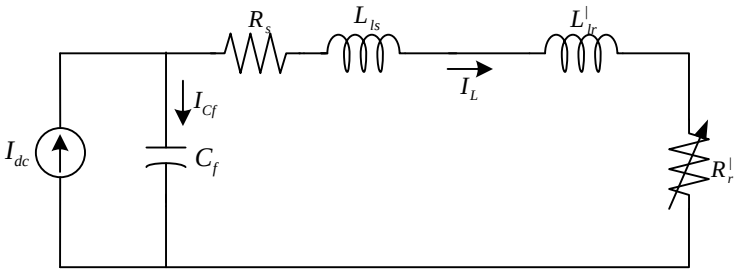

Figure 2.28: Equivalent circuit of CSI fed induction motor drive at higher frequencies

is,

Considering $L_{ls} + L_{lr'} = L$

At switching frequencies, most part of the current flows through the filter capacitor. Because, reactance offered by filter capacitance is low compared to leakage reactance. The relation between the capacitor filter current (I_{C_f}) and inductor current (I_L) is given in equations 2.68 and 2.69.

$$\frac{I_{C_f}}{I_L} = \frac{X_L}{X_{C_f}} \tag{2.68}$$

$$\frac{I_{C_f}}{I_L} = [(L_{ls} + L_{lr|})C_f]\omega_h^2 \tag{2.69}$$

where,

ω_h is harmonic frequencies.

Therefore to design filter capacitor following design rules are adopted,

a) Switching frequency ripple generated in PWM CSI fed drive is allowed to flow only through the capacitor.

b) The fundamental component of the current is allowed to flow through the machine.

Therefore, $\frac{I_{Cf}}{I_{lm}} < \frac{1}{10}$ (as obtained from equation 2.67) and $\frac{I_{Cf}}{I_{lm}} > 10$ (as obtained from equation 2.69) are considered to design the value of the filter capacitor.

$$C_f = \frac{1}{\omega^2 L_m} \tag{2.70}$$

2.8.1 Summary

This chapter focuses on Field oriented control technique of induction motor. Sensorless operation for estimating the speed of motor is discussed. Design of controllers and control algorithms is discussed in detail. Space vector pulse width modulation technique for current source inverter is analyzed. Design of filter is also discussed with appropriate equations.

CHAPTER 3

HARDWARE ORGANISATION FOR CSI FED INDUCTION MOTOR DRIVE

3.1 Introduction

Field oriented control technique involves in more number of mathematical operations and this makes analog implementation difficult. Therefore, field oriented control technique has been implemented in digital platform using micro-controller. The time taken by the digital micro-controller is very small and using digital approach, better results can be achieved.

The digital micro-controller used for implementing field oriented control of induction motor is Texas instrument's TMS320F28335. This chapter deals with the salient features of TMS320F28335 along with the other hardware employed such as protection card, analog signal conditioning card, inverter circuit and SCR based controlled rectifier.

3.2 Brief overview of TMS320F28335

This section gives a brief idea on salient features of digital signal controller (DSC) TMS320F28335 and the usage of micro-controller in implementation of FOC technique.

The two basic architectures of microprocessor are,

1. von Neumann architecture and
2. Harvard architecture.

In von Neumann architecture, salient features are shared memory space between code

and data and shared memory buses between code and data. Whereas in Harvard architecture, two independent memory spaces for code and data and two memory bus systems for code and data. Texas instrument's TMS320F28335 has Harvard architecture, i.e., seperate memory space and buses for code and data.

Figure 3.1 represents the block diagram of DSC TMS320F28335 and shows various components and bus architecture.

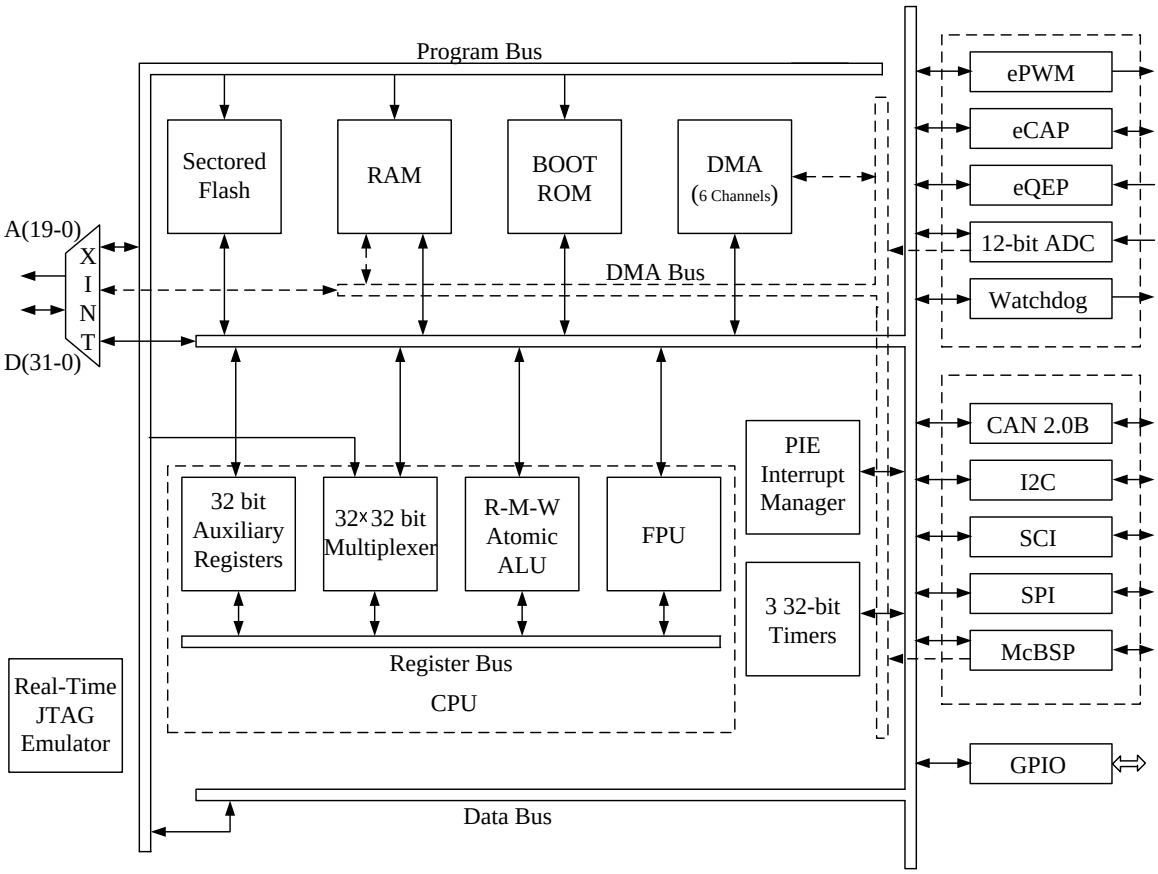

Figure 3.1: Block diagram of TMS320F28335

The functional units of TMS320F28335 are as follows,

- Internal and external bus system

TMS320F28335 has two independent buses namely,

a) Program bus and

b) Data bus.

This kind of architecture is known as Harvard architecture. In addition to the program and data buses, there is an additional bus known as register bus, for fast exchange of

data between its mathematical units.

- Central Processing Unit

The central processing unit (CPU) of TMS320F28335 has various features such as

a) 32 bit fixed and floating point DSP, 32 * 32 bit fixed point MAC

b) Additional 32 * 32 bit hardware floating point unit

c) Dual 16 *16 single cycle fixed point multiply and accumulate (MAC)

d) 32/64 bit saturation

e) Unique real-time debugging capabilities

- Internal memory sections

The memory map of TMS320F28335 is divided into two sub-modules,

a) Program space and

b) Data space.

There are several different types of memory available that can be used as program memory or data memory. These memory include independent sections of flash memory, Single Access RAM (SARAM), One Time Programmable memory (OTP) and Boot ROM. While the other includes boot software routines and trigonometric look-up tables.

- Control peripherals

The various control peripherals available in digital signal controller TMS320F28335 are enhanced pulse width modulation (ePWM) block, enhanced capture (eCAP) module and enhanced quadrature encoder pulse (eQEP) module.

- Communication channels

The various communication channels of TMS320F28335 are as follows,

a) Serial Communication Interface (SCI)

b) Serial Peripheral Interface (SPI)

c) Inter Integrated Circuit (I2C)

d) RS232 and

e) RS485.

- Direct Memory Access controller (DMA)

Direct Memory Access (DMA) unit allows a data transfer from source to destination without the interaction of CPU. DMA is an event based unit, i.e., it requires a peripheral interrupt trigger for the start of DMA transfer.

- Interrupt Management Unit (PIE) [6] and Core time unit

The Peripheral Interrupt Expansion (PIE) unit allows the user to specify the individual

interrupt service routines for a total of 96 internal and external interrupt events. All the 96 interrupt events share 14 maskable interrupts (INT1 to INT14) and 12 of them are controlled by PIE unit.

- Real-time Emulation unit

Real-time emulation unit performs various functions such as,

a) Analysis and breakpoint functions

b) Two hardware breakpoints per CPU

c) Real-time debug via hardware.

3.2.1 TMS320F28335 ePWM Module

Enhanced Pulse Width Modulation (ePWM) [4] is controlled by its own logic block. This logic can generate signals on different time events and to request various interrupt service routines from PIE of TMS320F28335. The central block of ePWM unit is 16 bit timer.

The block diagram of ePWM Module is shown in the figure 3.2.

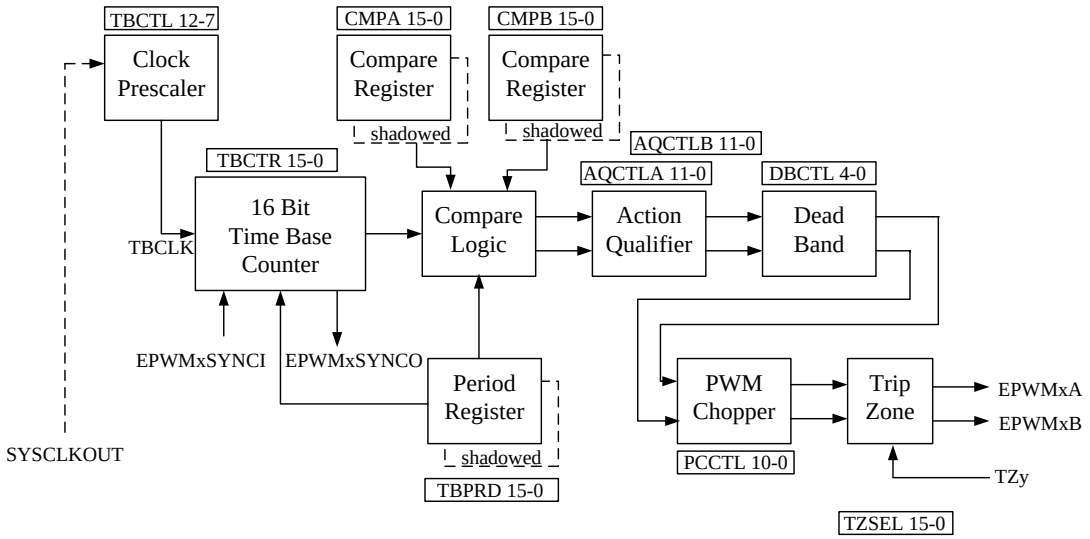

Figure 3.2: Block diagram for ePWM module of TMS320F28335

Brief description of various registers in ePWM module of TMS320F28335 are as follows,

Time Base Control Register

Time base control register is the master register for ePWM unit. It has various functions such as controlling the interaction between the micro-controller and JTAG emulator, phase direction, phase synchronization, time period, reducing the input frequency SYSCLKOUT and selecting the counter mode such as Up mode, Down mode, Up-down mode.

Action Qualifier Register

Action qualifier register takes a particular control action on the occurrence of 6 events, such as zero match, CMPA-up match, CMPB-up match, CMPA-down match, CMPB-down match and period match. The control actions are as follows,
a) set signal to high (rising edge)
b) clear signal to low (falling edge)
c) toggle the signal (high to low or low to high)
d) do nothing (ignore the event)

Event Trigger Register

Event trigger monitors various events such as time base counter matches zero, period, CMPA and CMPB. The event trigger pre-scaling logic can issue interrupt requests and ADC start of conversion at every event or at every second event or at every third event.

3.2.2 TMS320F28335 ADC Module

TMS320F28335 has 16 Analogue to Digital Conversion (ADC) channels. The processor is equipped with two sample and hold circuits which allows the conversion of two signals simultaneously. Also, the processor is equipped with auto-sequencer with a capability of 16 stages. The auto-sequencer of ADC automatically continues with the conversion of next signal after the conversion of present channel signal. ADC sequencer mode can set in two modes,

a) cascaded sequencer mode and

b) dual sequencer mode.

The block diagram for ADC module of TMS320F28335 [5] is shown in figure 3.3.

The relation between analog voltage and digital output is expressed as,

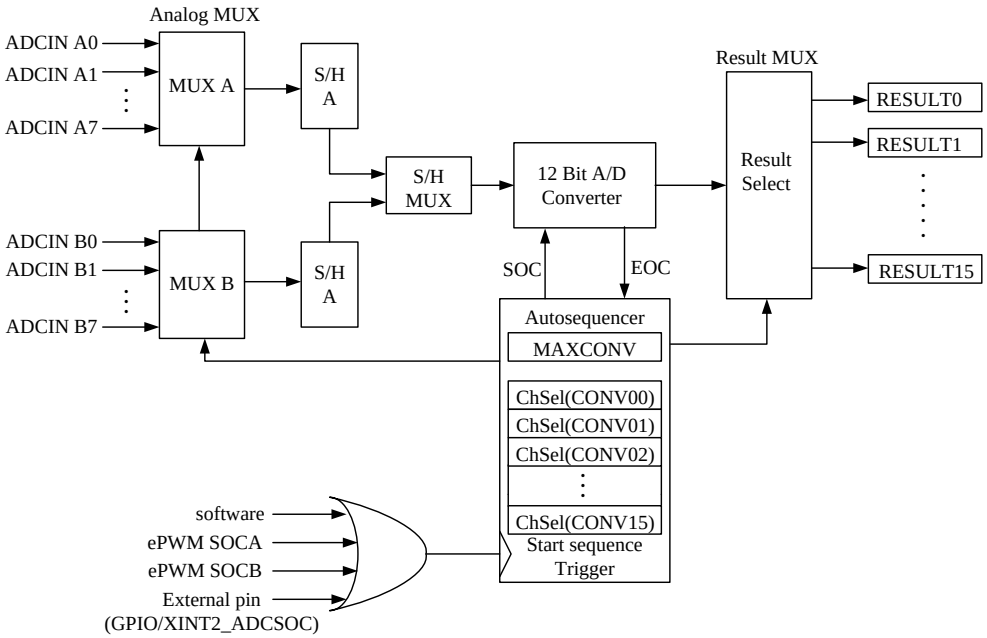

Figure 3.3: Block diagram for ADC module of TMS320F28335

$$V_{in} = \frac{3 * D}{4095} \tag{3.1}$$

Analog voltage of 0V gives the digital output of 0 and analog voltage of 3V gives the digital output of 4095. And the analog input voltage for the micro-controller should be within (0-3)V.

The ADC conversion can be started through 3 ways,

1. External trigger,
2. Software trigger and
3. ePWM trigger.

3.3 Voltage and current sensing

The inputs required for sensorless field oriented control technique are stator voltages and stator line currents of induction motor. The outputs from the sensors are also used for protection. Voltage and current sensors employed are based on the principle of Hall effect. The voltage sensors used are LV-25P, employed for sensing the stator line voltages and DC bus voltage. The current sensors used are LA-100P, employed for sensing stator line currents and DC link current.

3.4 Current source inverter module

The current source inverter is for converting DC current to alternating currents which are fed to the induction motor. The 3ϕ SCR based controlled rectifier gives DC voltage voltage which is converted into DC current by a heavy DC series inductor. This DC current is fed as input current for current source inverter. The switches used in current source inverter are IGBT (IXYS IXA12IF1200 HB) with a series diode. The ratings of IGBT switches are 1200V/20A. These switches are driven by Semikron SKYPER 32 PRO R IGBT gate drivers. The IGBT gate drivers provide isolation and shifts the voltage levels of gate pulses corresponding to turn ON and turn OFF of IGBT. The IGBT switches and diodes are properly mounted on heat sinks for thermal dissipation.

The capacitor bank is placed at the ac side of the inverter for filtering of harmonics and assisting in commutation of switching devices. The current source inverter with capacitor bank is shown in figure 3.6.

3.5 Protection card

The protection card safeguards the apparatus under fault conditions. Limiting values of stator line voltages, DC link voltage, stator line currents and DC link current are set using variable potentiometers. The voltage and current sensor outputs are continuously fed to the protection card. If any of the signals exceed the limiting values, corresponding protective measures are taken by turning ON all the switches of inverter and an

indication for corresponding fault is also provided through LED's. The protection card also provides an option for level shifting of gating pulses from (0-3.3)V to (0-15)V.

3.6 Analog signal conditioning card

The analog signal conditioning card conditions the bi-polar signals from voltage and current sensors to unipolar signals within the acceptable limits of micro-controller i.e., (0-3)V. These conditioned signals can be fed to ADC module of micro-controller. Analog signal conditioning card eliminates noise by employing differential line drivers. The output from voltage and current sensors are fed to signal conditioning card and their voltage levels should be within (-10V to 10V). This card also provides an option for level shifting of gating pulses from (0-3.3)V to (0-15)V. These level shifted signals are fed to gate drivers for further action.

3.7 Hardware setup

Sensorless field oriented control algorithms are implemented on a 0.75KW induction motor. Some of the photographs of drive setup and additional circuitry is presented in this section.

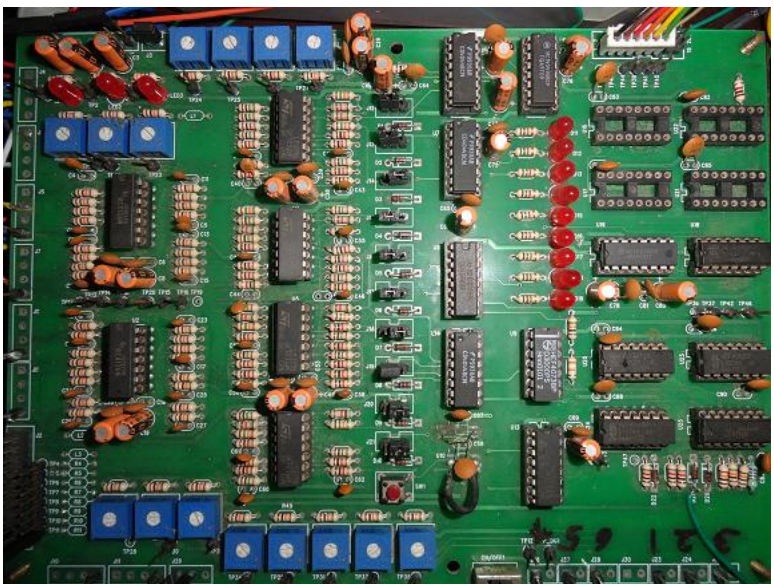

Figure 3.4: Protection card

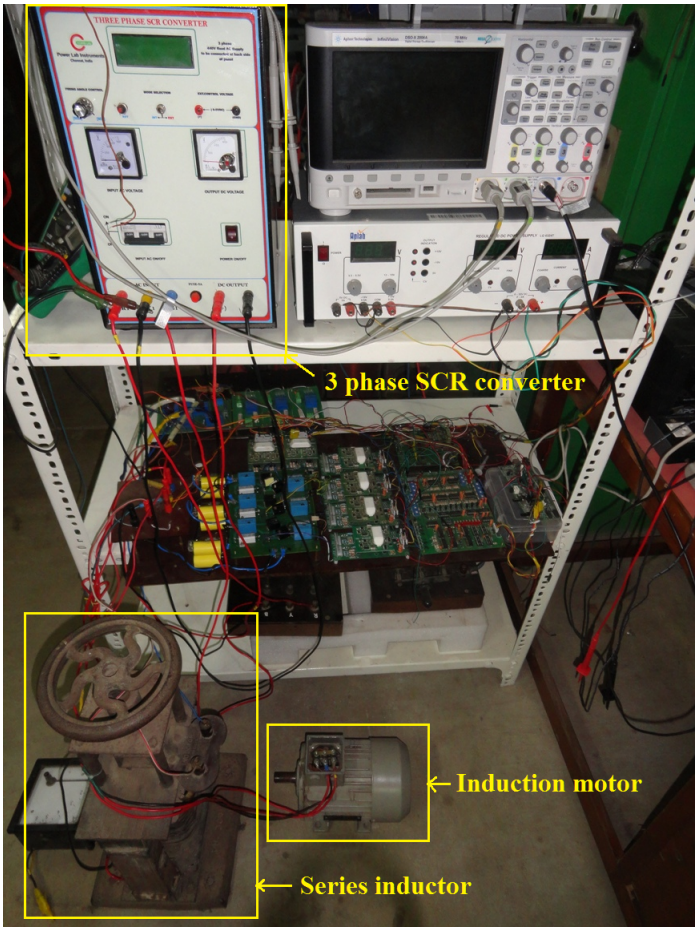

Figure 3.5: Hardware setup of CSI fed induction motor drive

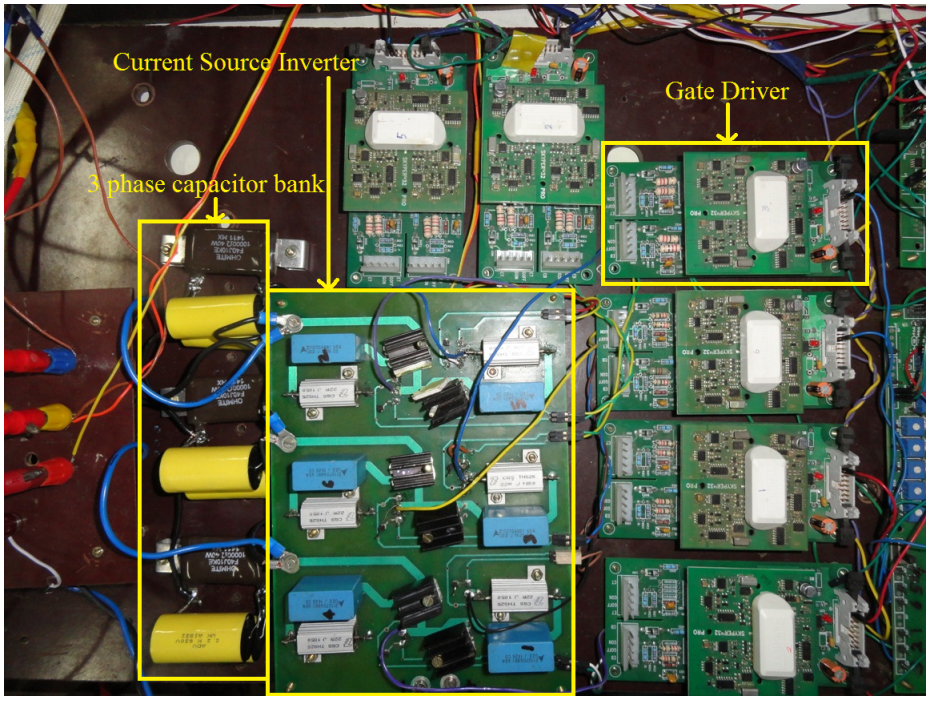

Figure 3.6: Current source inverter

3.8 Summary

This chapter focuses on hardware organisation of PWM-CSI fed induction motor drive. Overview of micro-controller TMS320F28335 and it's salient features are discussed. Functions of other hardware such as voltage and current sensors, CSI module, protection card and analog signal conditioning card is discussed.

CHAPTER 4

SIMULATION AND HARDWARE RESULTS OF CSI FED INDUCTION MOTOR DRIVE

4.1 Introduction

The simulation and hardware testing of PWM-CSI fed induction motor drive is carried out on a 0.75KW induction motor. This chapter gives the simulation and hardware results for PWM-CSI fed induction motor drive along with the descriptions.

4.1.1 Ratings of induction motor

The simulation of prototype CSI fed induction motor drive is carried on 0.75KW induction motor. The ratings of induction motor used in the simulation are given in Table 4.1,

Parameter	**Value**
Power	0.75KW
Current	1.8A
Powerfactor	0.81
Speed	1395rpm
Poles	4
Connection	star
Rotor type	Squirrel cage

Table 4.1: Ratings of induction motor

4.1.2 Parameters of induction motor

The parameters of induction motor are determined by conducting No load test and Blocked rotor test. The parameters of induction motor are given in Table 4.2.

R_s	$R_r^{\|}$	L_{ls}	L_{lr}	L_m
12.86Ω	12.86Ω	0.0575H	0.0575H	0.5159H

Table 4.2: parameters of induction motor

4.1.3 Controller parameters

The design of DC link current controller, flux controller and speed controller have been discussed in chapter 2. The various parameters such as proportional gain, integral gain, bandwidth and limiting values are given in Table 4.3.

Controller	$f_b(Hz)$	K_{pi}	T_{pi}	U_{max}	U_{min}
Flux controller	10	0.403	0.0403	6A	-6A
Speed controller	1	0.05	3.1056	5A	-5A
DC link current controller	0.2	396.5	5	1	-1

Table 4.3: Controller parameters

4.2 Simulation results

Simulation of CSI fed induction motor drive as shown in figure 2.10 has been done using Matlab Simulink. The objective of simulating the CSI fed induction motor drive is to evaluate performance and to assess the behavior of the drive. Simulating the model helps in identifying the various problems that can occur and can take necessary action to overcome the problems in real-time. Simulating the model also helps in designing parameters of the various controllers such as flux controller, speed controller and DC link current controller in real-time. The switching frequency of inverter is 3KHz. Following are the results for simulation of CSI fed induction motor drive.

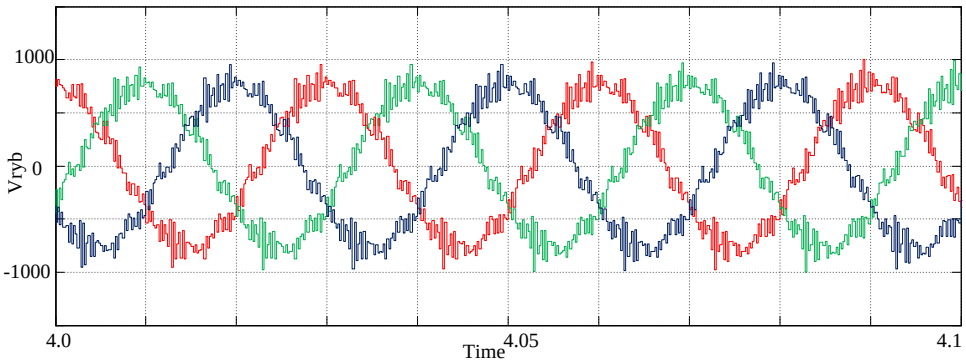

Figure 4.1: *Simulation result:*Steady stator line voltages of induction motor
Scale: X-axis: 0.01sec/div; Y-axis: 500V/div

Figure 4.1 represents the simulated steady state line voltages v_{ry} (red), v_{yb} (green) and v_{br} (blue) across the terminals of induction motor. The frequency of voltage waveform is 33Hz for the reference speed is 1000rpm. The voltage waveforms are pulse width modulated waveforms at the switching frequency of 3kHz. The fundamental component of voltage flows through the rotor magnetizing inductance and the switching component of voltage flows through the filter capacitance.

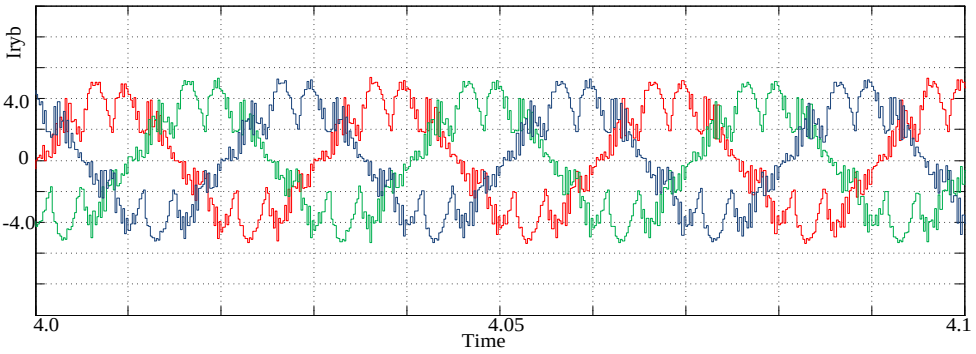

Figure 4.2: *Simulation result:*Steady stator line currents of induction motor
Scale: X-axis: 0.01sec/div; Y-axis: 2A/div

Figure 4.2 represents the simulated steady state line currents i_r (red), i_y (green) and i_b (blue) flowing into the induction motor. The frequency of current waveforms is observed as 33Hz which corresponds to the reference speed of 1000rpm. The current waveforms are pulse width modulated waveforms at the switching frequency of 3kHz. Similar to that of stator line voltages, the fundamental component of current flows through the rotor magnetizing inductance and switching component of current flows through the filter capacitor. The current ripple is high because of lower capacitance at the output ac terminals of inverter.

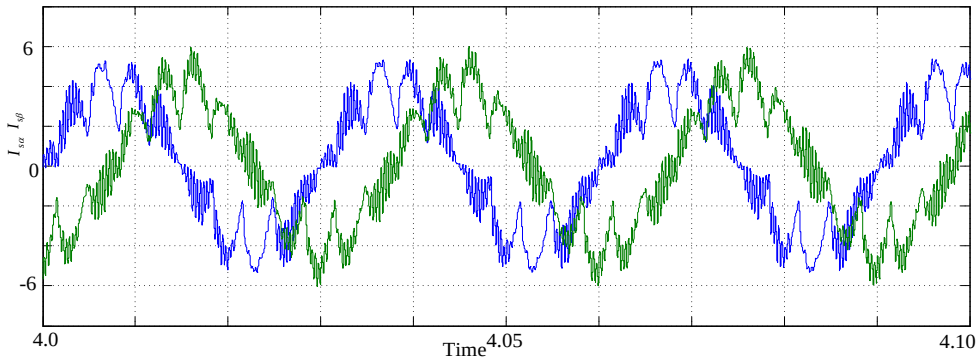

Figure 4.3: *Simulation result:*Alpha and beta components of stator line currents
Scale: X-axis: 0.01sec/div; Y-axis: 2A/div

Figure 4.3 represent the α (blue) and β (green) components of the stator currents of induction motor. α and β components can be derived from 3ϕ RYB components using Clarke's transformation. The frequency of the $\alpha\beta$ components is 33Hz. The waveforms are pulse width modulated the switching frequency of 3KHz. Ripple in α and β components of stator currents is due to lower capacitance at the output ac terminals of inverter.

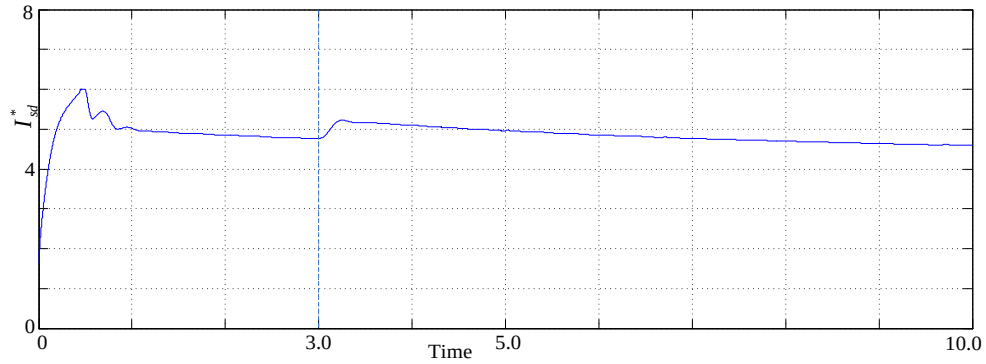

Figure 4.4: *Simulation result:*Output of flux controller (i^*_{sd})
Scale: X-axis: 1sec/div; Y-axis: 1A/div

Figure 4.4 shows a portion of variation of reference value of direct axis component of stator current (I^*_{sd}) i.e., the output of Flux controller. When the machine is loaded at time t = 3secs, the rotor magnetizing current (i_{mr}) is reduced. This lead to the increase in error signal generated by the reference value of rotor magnetizing current and actual magnetizing current. Thus leading to increase in reference value of direct axis component of stator current (I^*_{sd}). At steady state, the reference value of direct axis component of stator current (i^*_{sd}) equals rated rotor magnetizing current.

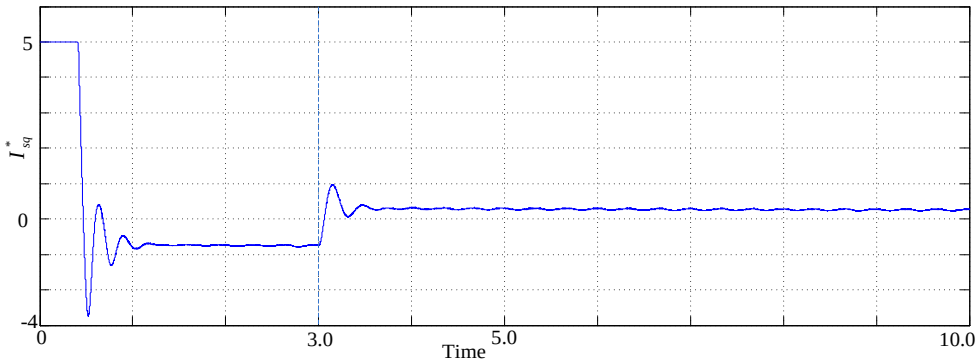

Figure 4.5: *Simulation result:*Output of speed controller (I^*_{sq})
Scale: X-axis: 1sec/div; Y-axis: 1A/div

Figure 4.5 gives the variation of reference value of quadrature axis component of stator current reference (I^*_{sq}) value i.e., the output of speed controller. The speed of the motor is greater than the reference speed of the speed controller in between the time t = 0 seconds and t = 3 seconds. Therefore, the speed controller generates negative value of quadrature axis component of stator current. The motor is said to be in regenerative operation during this period. When the machine is loaded at time t = 3 seconds, the speed of the induction motor falls below reference speed of speed controller. Therefore, the output of speed controller becomes positive after loading the machine.

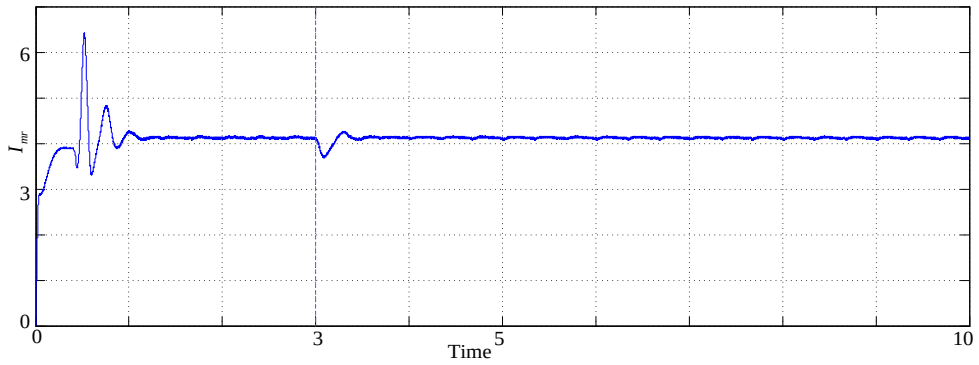

Figure 4.6: *Simulation result:*Variation of rotor magnetizing current (i_{mr})
Scale: X-axis: 1sec/div; Y-axis: 1A/div

Figure 4.6 shows the variation of rotor magnetizing current i_{mr} with respect to time. At steady state, rate of change of rotor magnetizing current tends to zero.Therefore, i_{mr} equals i_{sd}. When the machine is loaded at time t = 3 seconds, i_{mr} reduces because of reduction in speed. Immediately, the error signal generated by the reference value of rotor magnetizing current and actual magnetizing current increases. Thus resulting an increase in I^*_{sd} i.e., flux in machine.

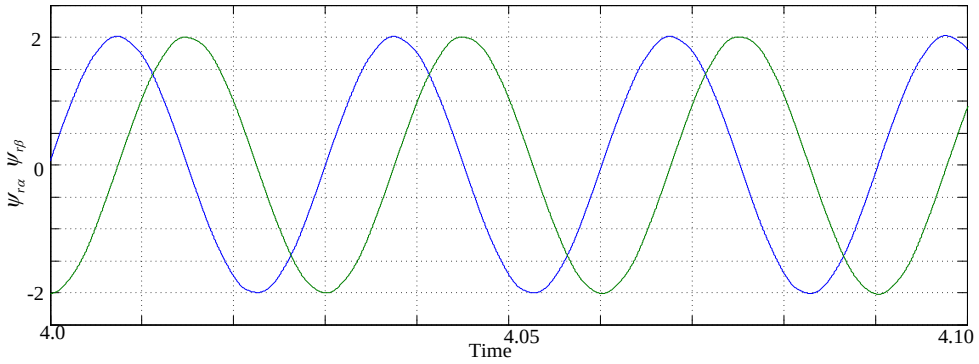

Figure 4.7: *Simulation result:* $\alpha\beta$ components of rotor flux linkages of induction motor
Scale: X-axis: 0.01sec/div; Y-axis: 0.5volt-sec/div

Figure 4.7 represents the α (blue) and β (green) components of rotor flux linkages at steady state. Using $\psi_{r\alpha}$ and $\psi_{r\beta}$, rotor flux position (ρ_{mr}) can be estimated. As α and β components of rotor flux linkage is varying sinusoidally and has a phase shift of 90^0, the rotor flux position will be varying linearly from $-\pi$ to π with the frequency corresponding to reference speed of speed controller.

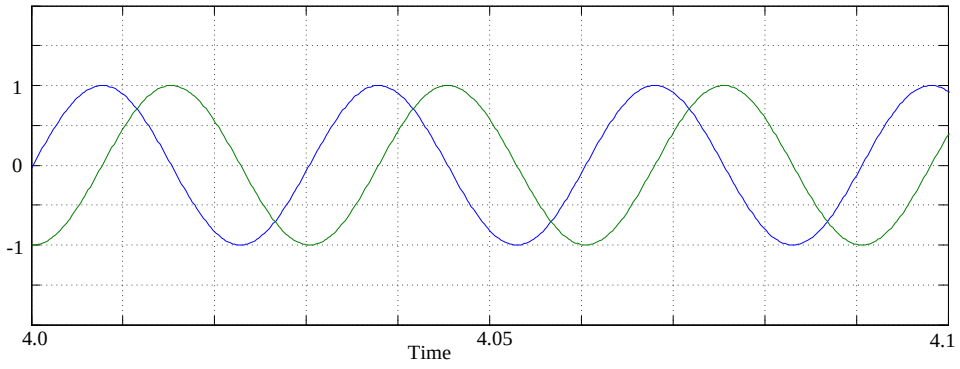

Figure 4.8: *Simulation result:*cos ρ_{mr} and sin ρ_{mr}
Scale: X-axis: 0.01sec/div; Y-axis: 0.5/div

Figure 4.8 shows the variation of cosine and sine of rotor flux position. $cos\rho_{mr}$ (blue) and $sin\rho_{mr}$ are determined using α and β components of rotor flux position. $cos\rho_{mr}$ (blue) and $sin\rho_{mr}$ (green) are sinusoidal signals and has a phase shift of 90^0 which implies rotor flux position is varying linearly from $-\pi$ to π in the form of ramp signal.

$$cos\rho_{mr} = \frac{\Psi_{r\alpha}}{\sqrt{\psi_{r\alpha}^2 + \psi_{r\beta}^2}}, \quad sin\rho_{mr} = \frac{\Psi_{r\beta}}{\sqrt{\psi_{r\alpha}^2 + \psi_{r\beta}^2}}$$

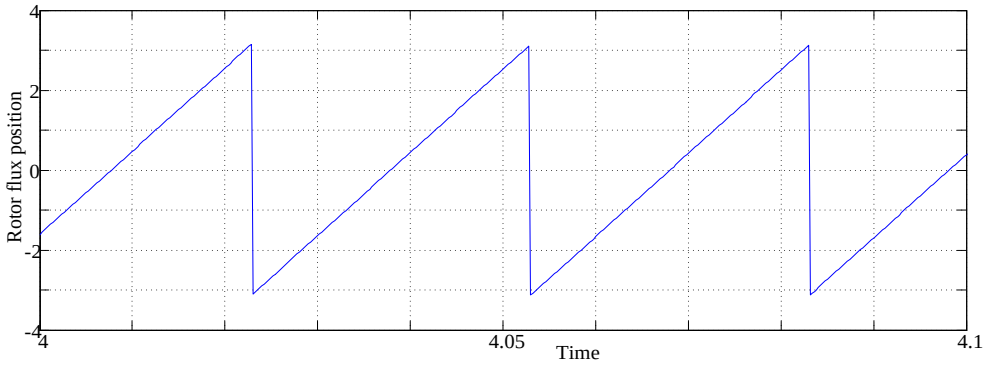

Figure 4.9: *Simulation result:*Estimated rotor flux position
Scale: X-axis: 0.01sec/div; Y-axis: 1radian/div

Figure 4.9 shows the estimated rotor flux position using sensorless field oriented control technique. The rotor flux position is determined using stator and rotor flux linkages. The stator and rotor flux linkages are found using stator voltages and currents. The block diagram for determining the rotor flux position is shown in figure 2.7. The rotor flux position is varying linearly form $-\pi$ to π with the frequency of 33Hz.

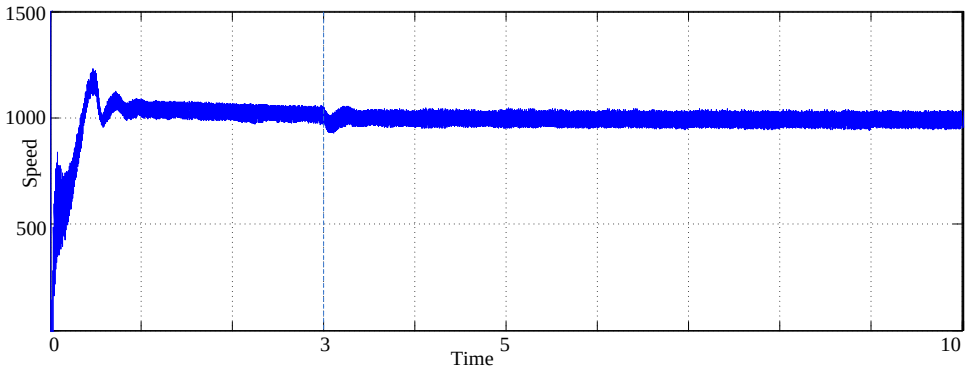

Figure 4.10: *Simulation result:*Estimated mechanical speed of induction motor
Scale: X-axis: 1sec/div; Y-axis: 500rpm/div

Figure 4.10 represents the estimated mechanical speed of the induction motor using sensorless control operation. As the speed is estimated using sensorless algorithm, the estimated speed curve is not smooth. The reference speed for the speed controller is 1000rpm. Therefore, from the figure 4.10, it is clear that the motor is running at the specified speed. When the motor is loaded at time t = 3secs, the speed of the motor is reduced. This results in the increase of error signal generated by the reference speed and actual speed of increases. Therefore, the reference value of quadrature axis component of stator current increases which in turn increases speed of the motor.

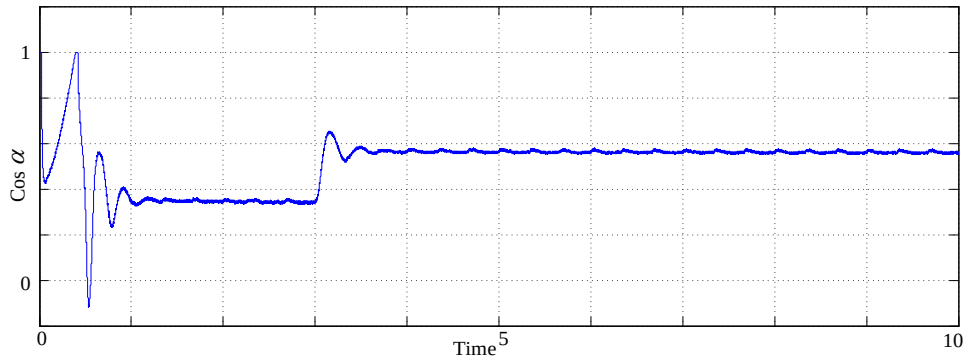

Figure 4.11: *Simulation result:Cosine of firing angle of 3ϕ SCR converter*
Scale: X-axis: 1sec/div; Y-axis: 0.2/div

Figure 4.11 shows the variation of cosine of firing angle of three phase SCR based controlled rectifier for controlling the DC link current. When the machine is operating under no load condition, the torque producing component of stator current required is very small. Therefore, the the firing angle of SCR converter is around 80^0, when the machine is operating under no-load condition. When the machine is operating under loaded condition, the torque producing component i.e., quadrature axis component of stator current (I_{sq}) increases. Thus the firing angle has been increased to around 55^0 under loaded condition.

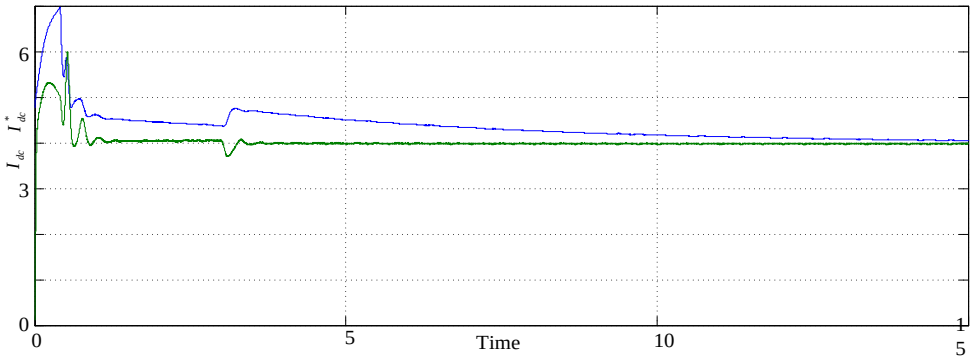

Figure 4.12: *Simulation result:*variation of actual DC link current (I_{dc}) with respect to the reference DC link current (I^*_{dc})
Scale: X-axis: 5sec/div; Y-axis: 1A/div

Figure 4.12 shows a portion of variation of actual DC link current(I_{dc}) (blue) with respect to reference value of DC link current(I^*_{dc}) (green). The DC link current can be controlled by controlling the firing angle of 3ϕ SCR converter. The actual DC link current has a peak value of 7A. From the figure 4.12, it is clear that the actual DC link current is tracking the reference value of DC link current.

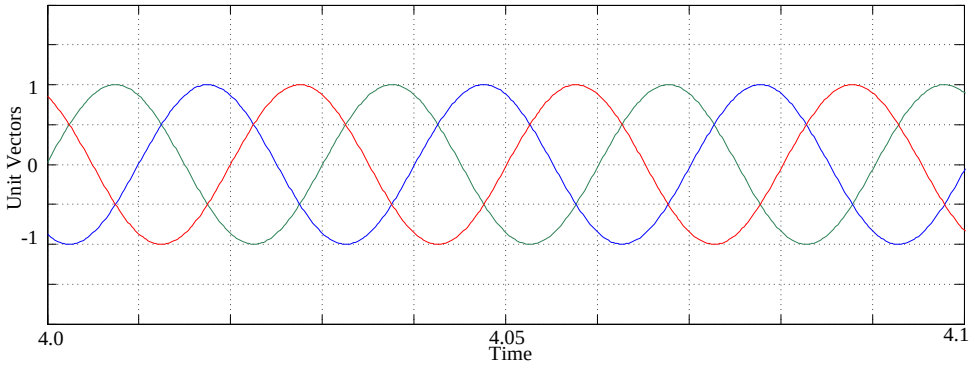

Figure 4.13: *Simulation result:*Unit vectors for generating PWM
Scale: X-axis: 0.0sec/div; Y-axis: 0.5/div

Figure 4.13 represents the three phase unit vectors derived from the outputs of flux and speed controllers. These unit vectors are used for generation of gating pulses for inverter. The PWM technique employed is space vector pulse width modulation.

4.3 Hardware results

PWM-CSI fed induction motor drive is developed on 0.75KW induction motor. The motor is running under no load condition with a reference speed is of 500rpm.

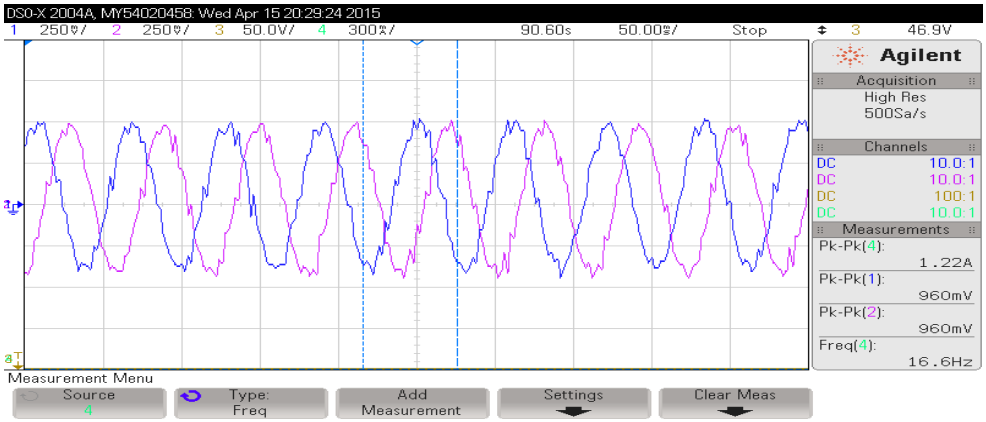

Figure 4.14: *Hardware result:*Steady state phase voltages of induction motor
Scale: X-axis: 50msec/div; Y-axis: 50V/div

Figure 4.14 represents the steady state phase voltages (R-phase (blue) and Y-phase (pink)) of induction motor. The voltage waveforms are pulse width modulated waveforms. The fundamental component of phase voltage flow through the rotor magnetiz-

ing inductance. Whereas the switching component of the voltage flows through the filter capacitor. Therefore, the voltage waveforms are sinusoidal in nature. The frequency of voltage waveforms is 16.6Hz which corresponds to speed of 500rpm.

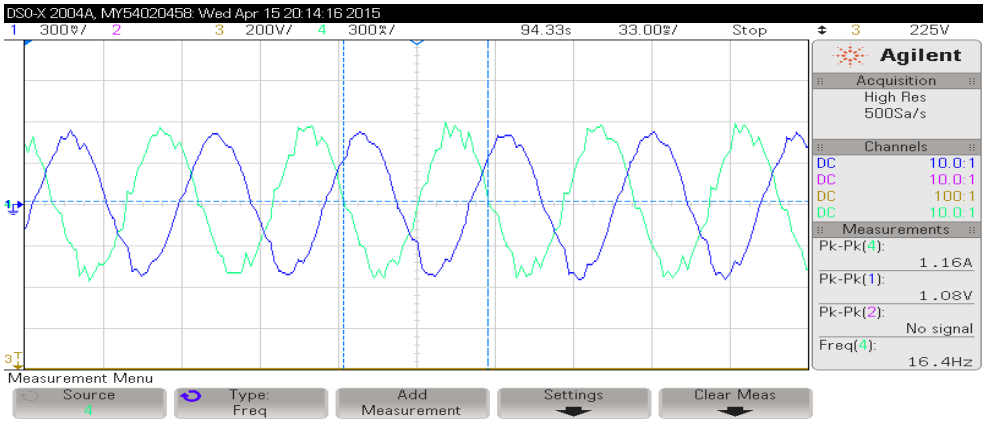

Figure 4.15: *Hardware result:*Steady state line currents of induction motor
Scale: X-axis: 33msec/div; Y-axis: 300mA/div

Figure 4.15 represents the steady state line currents (i_r (green) and i_y (blue)) of induction motor. The current waveforms are pulse widht modulated waveforms. Similar to the voltages, the fundamental component of the pulse width modulated current is allowed to flow through the rotor magnetizing inductance and the switching component of pulse width modulated current flows through the capacitor. Therefore, the line currents are sinusoidal in nature with a frequency of 16.4Hz.

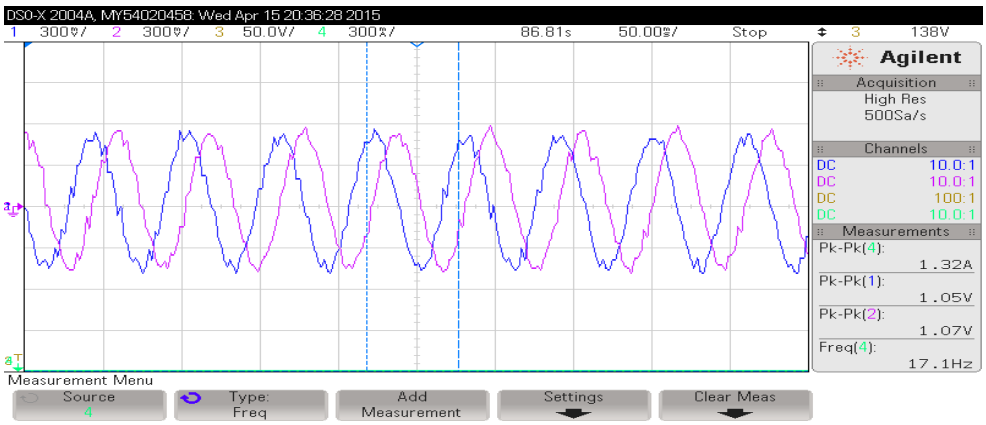

Figure 4.16: *Hardware result:*Alpha and beta components of the stator phase voltages of induction motor
Scale: X-axis: 50msec/div; Y-axis: 50V/div

Figure 4.16 represents the steady state alpha (α)(blue) and beta (β)(pink) components of phase voltages of induction motor. $\alpha\beta$ components are obtained from 3ϕ com-

ponents using Clarke's transformation. Alpha and beta components of stator phase voltages are sinusoidal in nature and has a phase shift of 90^0. The frequency of $\alpha\beta$ components of phase voltage is same as the phase voltages of the induction motor.

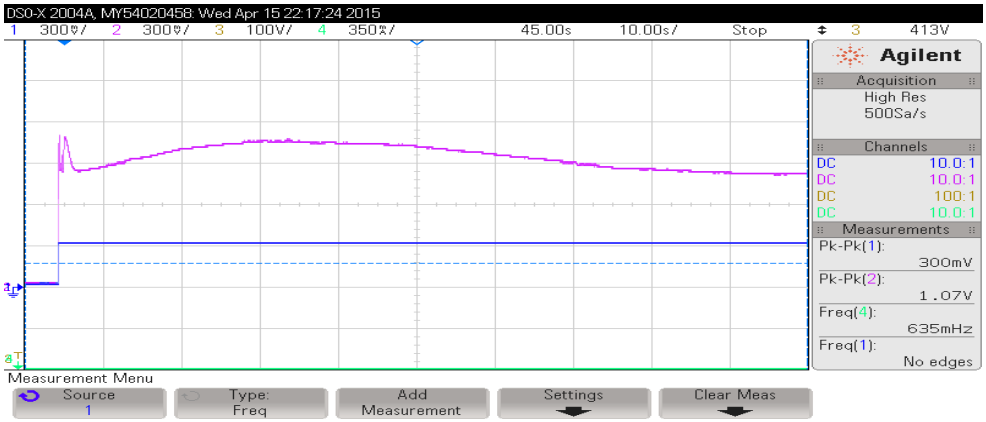

Figure 4.17: *Hardware result:*Outputs of Flux and speed controllers (I^*_{sd} and I^*_{sq})
Scale: X-axis: 10sec/div; Y-axis: 300mA/div

Figure 4.17 shows the variation of reference direct axis component of stator current (I^*_{sd})(blue) i.e., output of flux controller and variation of reference quadrature axis component of stator current (I^*_{sq})(pink) i.e., output of speed controller. As the reference rotor magnetizing current is high compared to the actual rotor magnetizing current, the output of the flux controller is immediately reaching the upper limit of the controller. As the torque required by the motor at starting is high, the reference value of quadrature axis component of induction motor is high. When the motor starts running and settles at reference speed, correspondingly I^*_{sq} varies and settles at a particular value.

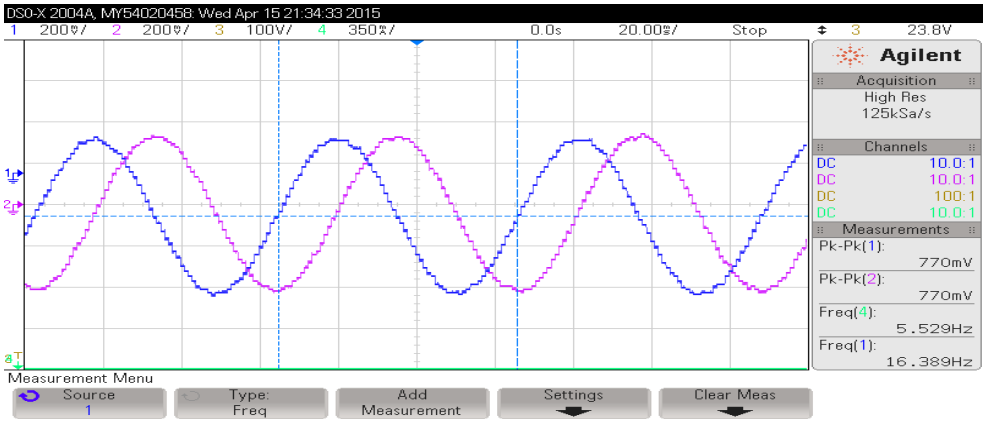

Figure 4.18: *Hardware result:*Alpha and beta components of stator flux linkages
Scale: X-axis: 20msec/div; Y-axis: 0.2mV-sec/div

Figure 4.18 represents the alpha(blue) and beta(pink) components of stator flux linkages, which can be determined by measuring the stator voltages and currents. The frequency of stator flux linkages is 16.4Hz. The DC offset present in the α component of stator flux linkage can be eliminated by passing through high pass filter or by a small negative feedback for the integrator.

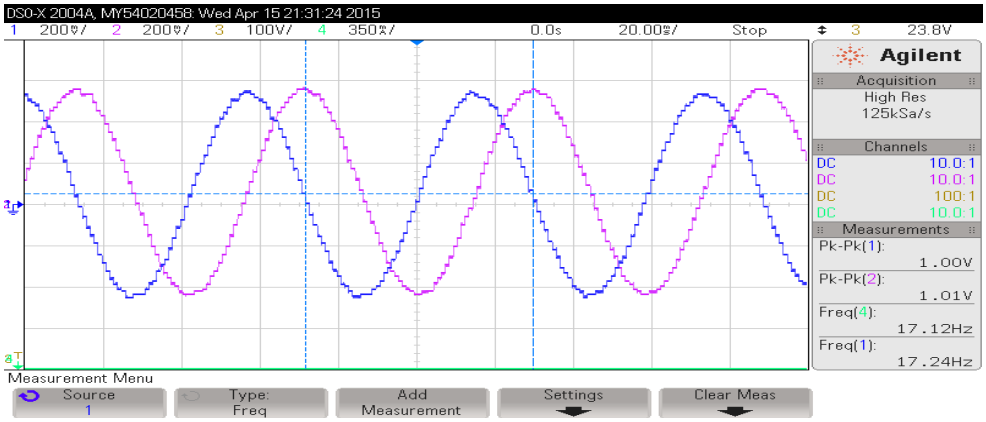

Figure 4.19: *Hardware result:*Alpha and beta components of rotor flux linkages
Scale: X-axis: 20msec/div; Y-axis: 0.2mV-sec/div

Figure 4.19 represents the α(blue) and β(pink) components of rotor flux linkages, which can be determined using alpha and beta components of stator flux and stator currents. The stator flux linkages can be found by using stator voltages and currents of induction motor. α and β components of rotor flux linkages are used for determining the position of rotor flux. The frequency of $\alpha\beta$ components of rotor flux linkage is around 17Hz.

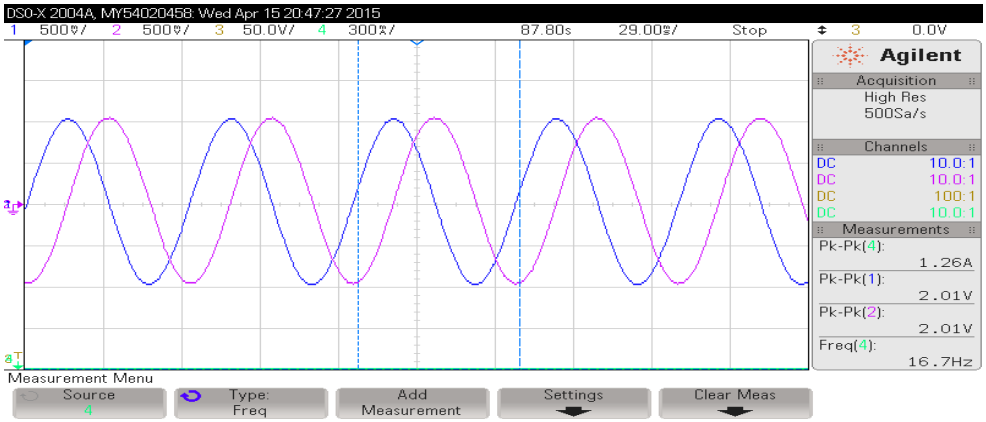

Figure 4.20: *Hardware result:*sine and cosine waveforms of rotor flux positions
Scale: X-axis: 29msec/div; Y-axis: 0.5/div

Figure 4.20 represents the sine(pink) and cosine(blue) waveforms of rotor flux position. The two signals shown have a phase shift of 90^0. These waveforms determine the rotor flux position instead of using inverse tan operation. Cosine of rotor flux position and sine of rotor flux position is defined as,

$$cos\rho_{mr} = \frac{\Psi_{r\alpha}}{\sqrt{\psi_{r\alpha}^2 + \psi_{r\beta}^2}}, \quad sin\rho_{mr} = \frac{\Psi_{r\beta}}{\sqrt{\psi_{r\alpha}^2 + \psi_{r\beta}^2}}$$

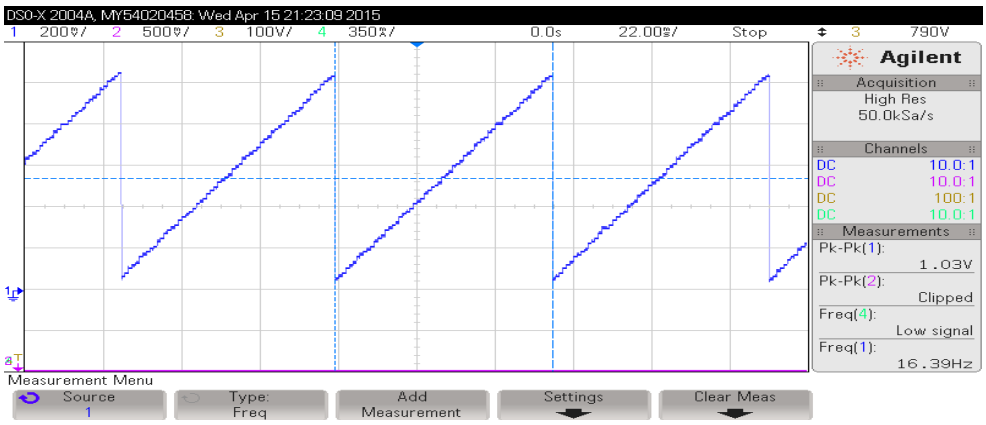

Figure 4.21: *Hardware result:*Estimated rotor flux position
Scale: X-axis: 22msec/div; Y-axis: 1.6rad/div

Figure 4.21 represents the rotor flux position which is estimated using $cos\rho_{mr}$ and $sin\rho_{mr}$ in sensorless operation. The rotor flux position helps in estimating the speed of motor. The rotor flux position is varying linearly from 0 to 2π at a frequency of 16.4Hz.

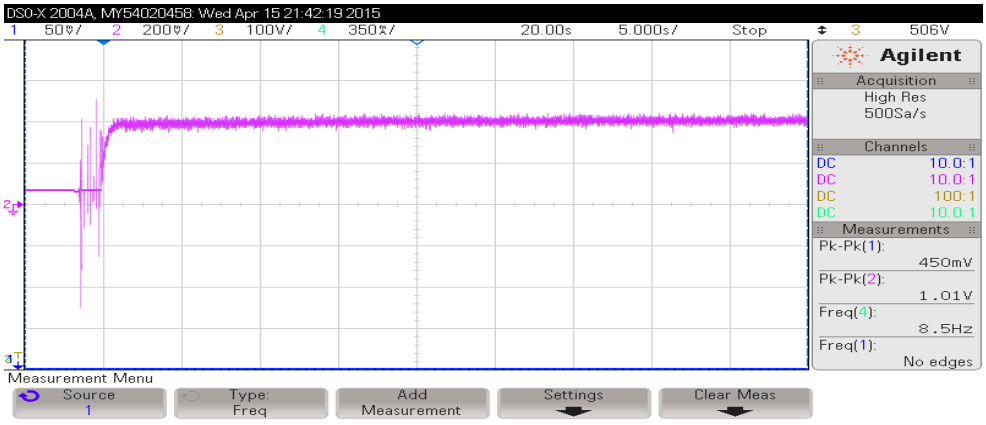

Figure 4.22: *Hardware result:*Estimated synchronous speed of induction motor
Scale: X-axis: 5sec/div; Y-axis: 250rpm/div

Figure 4.22 represents the estimated synchronous speed of induction motor which is determined by differentiating rotor flux position with respect to time. The algorithm

for finding the synchronous speed of induction motor is shown in figure 2.9. The actual speed of the motor can be estimated by subtracting slip speed from synchronous speed.

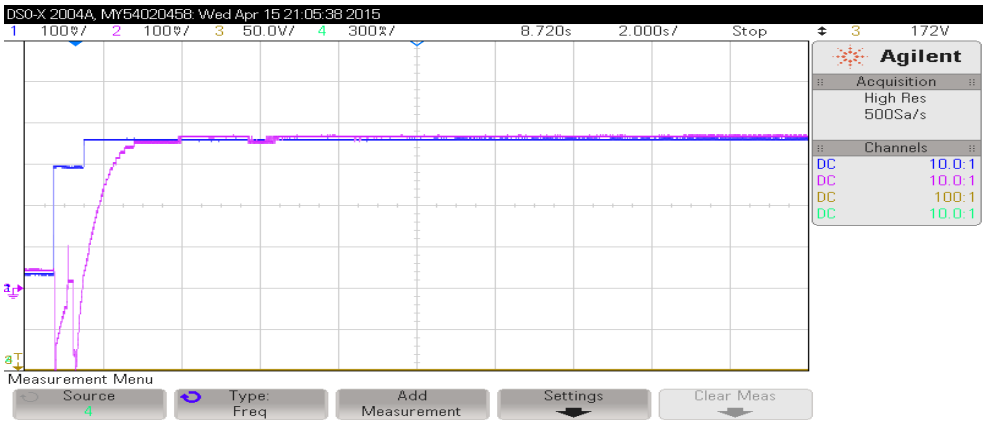

Figure 4.23: *Hardware result:*Estimated speed of motor correlated with reference speed
Scale: X-axis: 2sec/div; Y-axis: 0.5/div

Figure 4.23 shows the correlation between actual speed(pink) of motor and reference speed(blue) of speed controller. The drive is not started for the initial 0.8 seconds of operation and during this period the offsets of sensed voltages and currents are determined. During this period, the reference speed for the speed controller is 400rpm. The reference speed of the speed controller is changed to 500rpm as soon as the gating pulses are fed to the inverter switches.

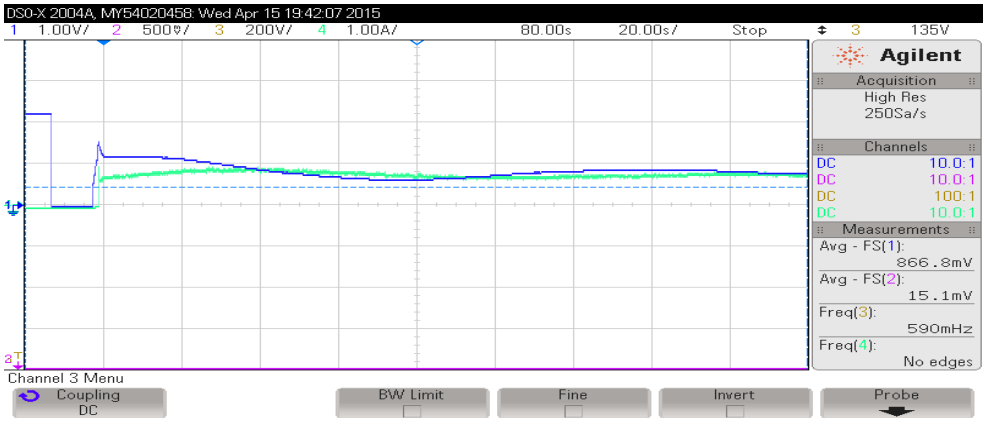

Figure 4.24: *Hardware result:*Correlation between I^*_{dc} and I_{dc}
Scale: X-axis: 20sec/div; Y-axis: 0.5/div

Figure 4.24 shows the correlation between actual DC link current (I_{dc})(blue) and reference DC link current (I^*_{dc})(green). By varying firing angle of SCR converter, I_{dc} tracks I^*_{dc}. I^*_{dc} is tracking I_{dc}, but at a slower rate.

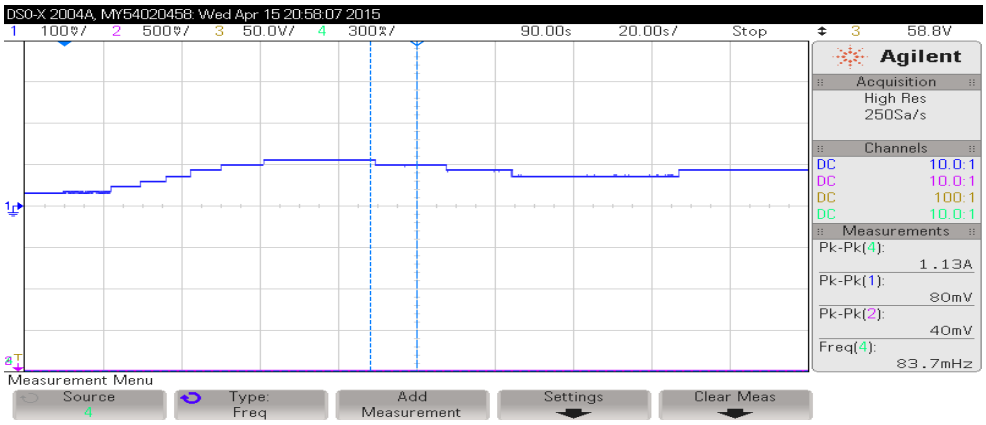

Figure 4.25: *Hardware result:*Variation of cosine of firing angle of SCR converter
Scale: X-axis: 20sec/div; Y-axis: 0.5/div

Figure 4.25 shows the variation of cosine of firing angle of three phase SCR based converter. This allows actual DC link current to track reference DC link current.

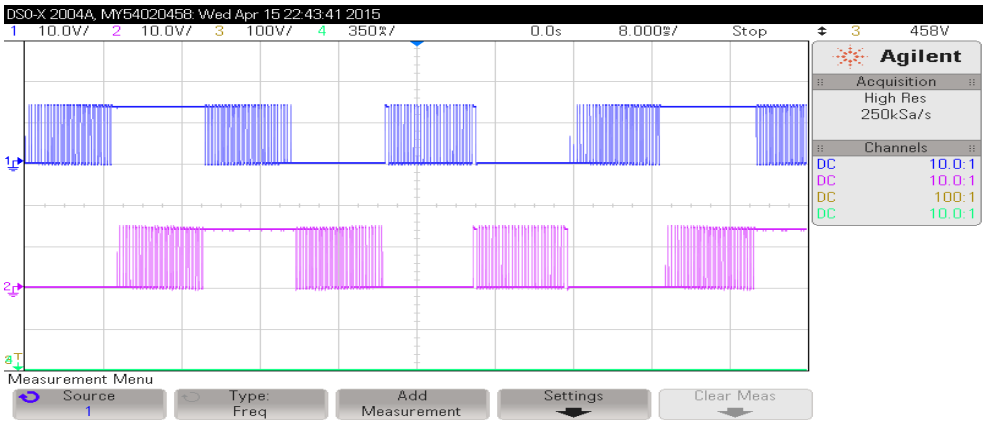

Figure 4.26: *Hardware result:*Gating pulses for switches 1 and 2 of CSI
Scale: X-axis: 8msec/div; Y-axis: 0.5/div

Figure 4.26 shows the gating pulses for IGBT switches numbered 1 (blue) and 2 (pink) of current source inverter (CSI). The switching frequency of the inverter switches is 3KHz.

CHAPTER 5

CONCLUSION

5.1 Summary of present work

The sensorless field oriented control of induction motor was successfully implemented on 0.75 kW induction motor. The reasons for choosing current source inverter instead of voltage source inverter are discussed in detail in this report. The theoretical concepts required for implementing the CSI fed induction motor drive such as Field oriented control of induction motor, sensorless operation for estimating the speed of motor using stator voltages and currents are discussed. Field oriented control technique of induction motor helps in achieving decoupled torque and flux control. This report discusses control algorithms for different controllers such as flux controller, speed controller and DC link current controller. Space vector pulse width modulation technique is analyzed and is implemented for better dynamic response. Design of filter is done analytically in detail.

The proposed field oriented control technique is implemented using Texas instrument's TMS320F28335 digital signal controller. This report gives brief introduction to TMS320F28335 and it's salient features such as ADC module, ePWM module and other modules. Brief description of voltage and current sensing, current source inverter, protection card and analog signal conditioning card is discussed.

The simulation of proposed drive is done in Matlab Simulink and the simulation results along with descriptions are presented for reference speed of 1000rpm. The complete hardware is developed in laboratory and the hardware results along with descriptions are presented for reference speed of 500rpm. Higher speeds are not achieved because of the limitation of SCR converter. This can be overcome by replacing SCR converter with current source rectifier.

5.2 Future scope of work

The 3ϕ SCR converter can be replaced with PWM current source rectifier for better controllability, reliability of CSI fed induction motor drive. This also enhances the power quality and dynamic response of the drive. This drive is intended for sub-sea mining application. Therefore, modeling of long transmission cable and evaluation of performance of the drive can be carried out.

REFERENCES

[1] Bin Wu, *High-power Converters and AC Drives*, Wiley-Interscience, December 2005.

[2] B. K. Bose, *Power Electronics and Motor Drives: Advances and Trends*, Elsevier Science, 2010.

[3] Parthiban P., Pramod Agarwal, Srivastava S.P., *A Simplified Space-Vector Modulated Control Scheme for CSI fed IM drive*, PEDES, 2006.

[4] Texas Instruments, *TMS320x2833x, 2823x Enhanced Pulse Width Modulator (ePWM) Reference Guide (Rev. A)*, July 2009.

[5] Texas Instruments, *TMS320x2833x, 2823x Analog-to-Digital Converter (ADC) Module Reference Guide (Rev. A)*, October 2007.

[6] Texas Instruments, *TMS320x2833x, 2823x Interrupt System Reference Guide (Rev. A)*, April 2010.